Light induced cell death in the cancer cell line AY-27: Modes of cell death after red-light hexylaminolevulinate photodynamic therapy and effects of fractionated light delivery

Ingvild Kinn Ekroll

Department of Physics — NTNU 2009

Description of thesis

Student:	Ingvild Kinn Ekroll
Written at:	Department of Physics, NTNU
Period:	January 20 – June 16, 2009
Supervisor:	Anders Johnsson, Department of Physics, NTNU
English title:	Light induced cell death in the cancer cell line AY-27: Modes of cell death after red light hexaminolevulinate photodynamic therapy and effects of fractionated light delivery
Norwegian title:	Lysindusert celledød i kreftcellelinjen AY-27: Celledødsmetoder etter hexaminolevulinsyre fotodynamisk terapi med rødt lys, og effekter av fraksjonert lysbehandling

Preface

This work marks the end of five years of studies, all of which have provided me with new experiences and knowledge — often about phenomena I had never heard of before.

When I started my specialization in Biophysics and Medical Technology, I had never heard of photodynamic therapy. But when I did, its great potential and the seemingly simple mechanisms fascinated me. After working with the subject for some time, it is still truly fascinating, but it no longer appears simple. In fact, as the mechanisms in PDT are steadily uncovered, the diversity and complexity of it all can seem overwhelming.

My understanding of the subject is based on contributions from many people, and some acknowledgements are in order:

I would like to thank my supervisors at the Department of Physics, Anders Johnsson and Thor Bernt Melø, for providing the opportunity to write a master's thesis about PDT, and for all their help.

Odrun Arna Gederaas and Linda Helander at the Department of Cancer Research and Molecular Medicine has given invaluable help in all aspects of the work with this thesis, and deserve a big thank you.

Kristin Sæterbø has answered all sorts of questions related to working with cells, and has been a great help in planning and performing the experiments.

A special thanks to Kristine Feness for providing company in the darkness of the lab and extra hands when needed, and to Erlend Magnus Viggen for proofreading the manuscript.

Finally, Jørgen, my storage of optimism, thanks to you!

Abstract

This study aimed to further investigate light induced cell death in the rat bladder cancer cell line AY-27 after incubation with hexylaminolevulinic acid; a treatment known as photodynamic therapy (PDT). Flow cytometry and confocal microscopy was used to examine the modes of cell death after treatment. Results from flow cytometry one hour after light delivery was used to establish dose-response curves for viable, apoptotic and necrotic cells. These curves indicate that necrosis is the dominant mode of cell death in our study.

The LD_{50} dose, found from the survival curve, was used in studies of fractionated and split light delivery. No altered effect was detected between treatment with fractionated and continuous light delivery. The survival in split-dose experiments seemed to depend on conditions before irradiation, but they otherwise gave the same amount of cell death as fractionated or continuous light delivery. These results were confirmed both by flow cytometry and by measurements of mitochondrial activity, as found by the MTT assay.

Sammendrag

Dette arbeidet hadde som målsetting å bidra til en større forståelse av lysindusert celledød i kreftcellelinjen AY-27 etter inkubasjon med hexylaminolevulinsyre; også kalt fotodynamisk terapi (PDT). Flowcytometri og konfokalmikroskopi ble brukt til å kartlegge mekanismer av celledød etter slik behandling, og data fra flowcytometri én time etter belysning ble brukt til å etablere dose-respons-kurver for viable, apoptotiske og nekrotiske celler. Resultatene indikerer at celledød ved nekrose dominerer i denne studien.

LD_{50}-dosen, funnet fra overlevelseskurven, ble brukt i studier av fraksjonert og splittet lysbehandling. Det ble ikke funnet noen endret effekt mellom fraksjonert og kontinuerlig lysbehandling. Overlevelsen etter belysning i to like intervaller avbrutt av en mørkeperiode på fem minutter ser ut til å avhenge av betingelser før belysning, men ser ellers ut til å gi samme overlevelse som fraksjonert og kontinuerlig belysning. Disse resultatene ble bekreftet både ved bruk av flowcytometri og måling av mitokondriell aktivitet, funnet ved hjelp av MTT-metoden.

Abbreviations

ALA	Aminolevulinic acid
ALAS	Aminolevulinic acid synthase
Ax	Annexin V Fluos
BCC	Basal cell carcinoma
BCNU	1,3-bischloroethyl-nitrosourea
BPD	Benzoporphyrin derivative monoacid ring A (verteporfirin)
dH_2O	Distilled water
DNA	Deoxyribonucleic acid
EDTA	Ethylenediaminetetraacetic acid
FBS	Fetal bovine serum
GSH	Reduced glutathione
HAL	Hexylaminolevulinate
HEPES	4-(2-hydroxyethyl)-1-piperazineethanesulfonic acid
HpD	Hematoporphyrin derivative
JC-1	5,5',6,6'-tetrachloro-1,1',3,3'-tetraethylbenzimidazolocarbocyanine iodide
LD_{50}	Lethal dose, 50%
MAL	Methylaminolevulinate
MTT	3-4(4,5-demethylthiazol-2-yl)-2,5 diphenyltetrazolium bromide
m-THPC	Meta-tetra hydroxyphenyl chlorine (temoporfin)
PDT	Photodynamic therapy
PI	Propidium iodide
PpIX	Protoporphyrin IX
RNA	Ribonucleic acid
ROS	Reactive oxygen species
TCC	Transitional cell carcinoma
YO-PRO-1	Quinolinium, 4-0(((3-methyl-2(3H)-benzoxazolylidene)methyl)-1-03-(trimethylammonio)propyl)-, diiodide

Contents

List of Figures

Chapter 1

An introduction to PDT and its applications

1.1 Photodynamic therapy

Photodynamic therapy (PDT) as we know it today has only been developed in the last century, but light has been used for therapeutic purposes for more than three thousand years. Examples have been found both in ancient Egyptian, Indian and Chinese civilizations, where light was used to treat diseases such as psoriasis, rickets and skin cancer [1].

At present, PDT is mostly used in connection with different types of cancer (as seen in Table 1.1), but can also be used with bacteria. In the latter case PDT could be an alternative to antibiotic treatment and thus be advantageous when antibiotic resistant bacteria strains develop. Among possible targets of antimicrobial PDT are acne vulgaris, periodontal diseases and infected wounds [2, 3].

Photodynamic therapy utilizes an interaction between light and molecular oxygen in cells or tissue, mediated by a chemical substance called a *photosensitizer*. These three components are all needed to get a photodynamic effect. The mode of action is illustrated in Figure 1.1. The photosensitizer can absorb a photon leading to the excitation of one of its electrons. *Reactive oxygen species* (ROS) are formed when the photosensitizer deexcites in a reaction with oxygen. These ROS can interact with neighbouring molecules, such as lipids and proteins, and by this cause cell injury.

PDT has several advantages over traditional cancer treatment modalities such as surgery, ionizing radiation and chemotherapy. It is minimally invasive, has low mutagenic potential, low systemic toxicity and is selective of cancerous over normal tissue, due to the preferential accumulation of the photosensitizer in tumor tissue and light exposure only to the cancerous area [2–4].

As can be seen in Table 1.1, the combination of a photosensitizer and light is also used in cancer diagnosis; *fluorescence diagnosis* (FD) or *photodynamic diagnosis* (PDD), where fluorescence from excited photosensitizers is used to detect cancer tissue. There is also much research focusing on *photochemical internalization* (PCI), a method for cytosolic delivery of drugs that are trapped in endosomes and lysosomes. In PCI, the

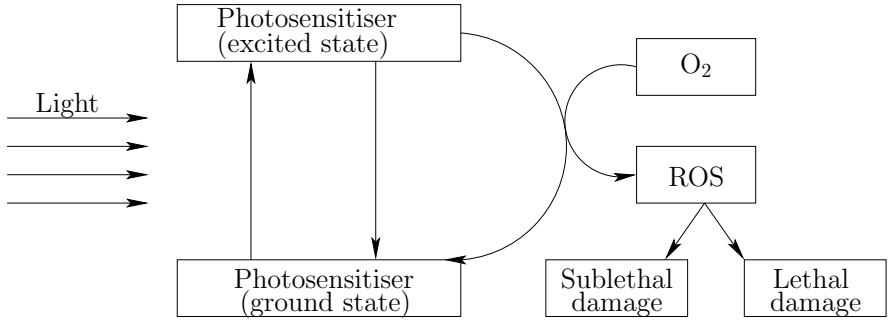

Figure 1.1: A simple illustration of the principle of photodynamic treatment. Light is absorbed by the photosensitizer. If the photosensitizer deexcites during a reaction with molecular oxygen, reactive oxygen species are generated. The ROS can induce lethal or sublethal damages to a cell by oxidatively damaging lipids or proteins in the cell.

photosensitizer will first adsorbe to the plasma membrane before it is endocytosed into the membranes of the endocytic vesicles. The drugs trapped inside will enter the cytosol when the membranes of the endosomes or lysosomes are ruptured following illumination with an appropriate light source [3].

Table 1.1: Approved photosensitizers for the use in PDT and FD. Adapted from [2, 3]

Trade name	**Abbreviation**	**Producer**	**Indication**
Photofrin	HpD	Axcan Pharma	Barret's Oesophagus, Cervical dysplasia, Cervical cancer, Lung cancer, Oesophageal cancer, Gastric cancer, Bladder cancer
Visudyne	BPD	Novartis	Age-related macular degeneration
Foscan	m-THPC	Biolitec Pharma	Head and neck cancer
Levulan	ALA	DUSA Pharmaceuticals	Actinic keratosis, BCC
Metvix	MAL	Photocure ASA	Actinic keratosis, BCC
Hexvix	HAL	Photocure ASA	FD of bladder cancer

1.2 Bladder cancer

According to Parkin *et al.* [5], urinary bladder cancer causes 130 000 deaths every year worldwide. 90 percent of these deaths are caused by transitional cell carcinomas (TCC)[1] [6]. Smoking is the most important risk factor for bladder cancer, probably due to the high content of carcinogenic arylamides in cigarette smoke [6, 7].

As bladder cancer is the fourth most common tumor among males in USA and the ninth most common cancer worldwide [6], an additional or alternative treatment modality to surgery, endoscopic resection, chemotherapy and immunotherapy is most welcome.

Photodynamic therapy could be one such alternative if treatment protocols are optimized. Superficial urinary bladder cancer is suited for PDT, because the bladder can easily be illuminated using optical fibers, it is more translucent than other human tissues [8] and the photosensitizer can be delivered either intravenously or intravesically [7], which motivates further research on PDT using urinary bladder cancer cells.

The experiments in this project are performed on rat bladder transitional cell carcinoma cells (AY-27). Results can with relative ease be further investigated *in vivo*, as there are groups at NTNU performing studies where the AY-27 cell line is used to induce TCC in rats, e.g. the work of Larsen *et al.* [7].

1.3 Purpose of study

1. Study the modes of cell death in the cancer cell line AY-27 after treatment with the photosensitizer hexyl-aminolevulinic acid (HAL) and red light.

2. Compare flow cytometry and confocal microscopy for quantitative measurements of cell death after red light HAL-PDT.

3. Study effects of fractionating the light delivery in red light HAL-PDT.

[1] Transitional cells form the lining of the bladder, the transitional epithelium

Chapter 2

Background

2.1 Photophysical mechanisms in PDT

A photon-excited photosensitizer molecule has several ways of returning to its ground state. These processes can be visualized using a Jablonski diagram as shown in Figure 2.1. Radiative processes are represented by straight arrows, whereas nonradiative processes are represented by dashed arrows.

The different possible transitions between molecular energy states have different transition probabilities per unit time, and are characterized by transition rate constants. The lifetimes of the different energy states are defined using these constants. Taking fluorescence as an example, the fluorescent lifetime τ_f equals $1/k_f$, where k_f is the probability per unit time for the molecule to deexcite through fluorescence.

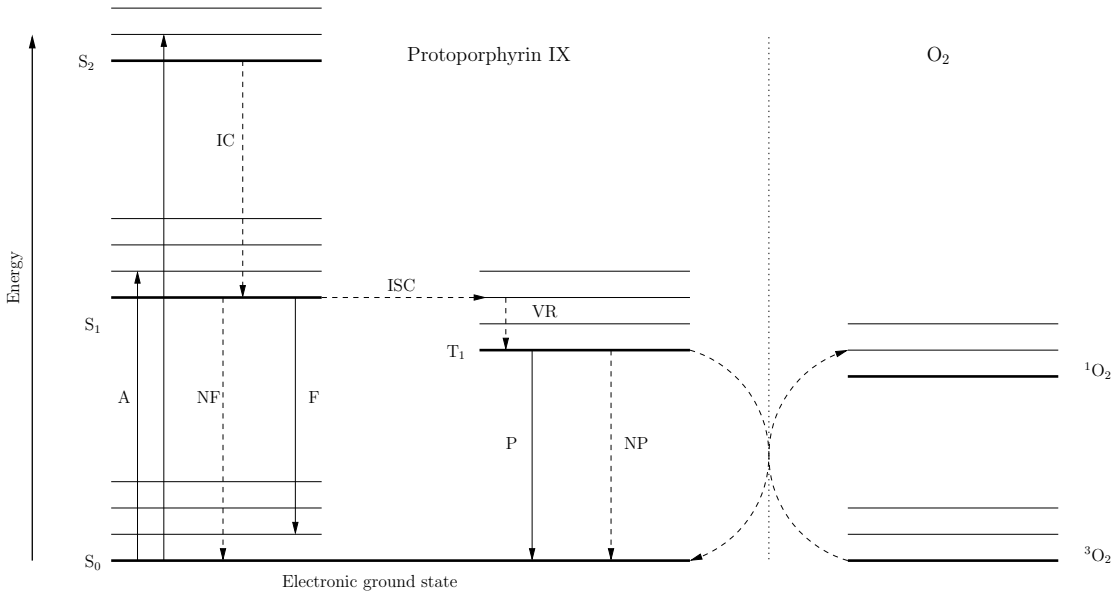

Figure 2.1: A Jablonski diagram visualizing transitions between energy states in a molecule. The processes shown are absorption (A), fluorescence (F), phosphorescence (P), non-phosphorescence (NP), intersystem crossing (ISC), internal conversion (IC), vibrational relaxation (VR) and energy exchange between two triplet state molecules. Other processes can also occur.

Absorption (A): Photons of different frequencies with energy $h\nu$ can be absorbed when the molecule is in its ground state. The photons are selectively absorbed depending on the energy levels available to the molecule.

Internal conversion (IC): A non-radiative transition between electronic states of the same spin multiplicity. This is the main transitional mechanism between S_2 and S_1 and the lifetime of the upper energy level is short, typically of magnitude 10^{-14}s.

Vibrational relaxation (VR): Excess vibrational energy is dissipated into heat, leaving the molecule in the lowest vibrational level within the same spin state.

Fluorescence (F): Emission of light following a transition from a singlet excited state to a singlet ground state. This is a "spin allowed" transition, thus having a short lifetime, of order 10^{-9} s.

Intersystem crossing (ISC): A transition between states of different spin multiplicity, a socalled "spin-forbidden" transition, but promoted by spin-orbit coupling. In porphyrins the k_{isc} is quite large, about 70 % of the excited molecules will enter a triplet state. The presence of molecular oxygen will increase this number of triplet state molecules [9].

Phosphorescence (P): Emission of light following a transition from a triplet excited state to a singlet ground state, or from a singlet excited state to a triplet ground state. This is also a "spin-forbidden" transition, and the lifetime of the triplet

state will be longer than the fluorescence lifetime, up to seconds (typically 10^{-3} s - 1 s). This increases the probability that the excited molecule will interact with other molecules by transfer of energy [9, 10].

A molecule can have several possible electron configurations, giving different total energies. In the ground state, the electrons will occupy the molecular orbitals giving the lowest energy for the molecule. The ground state of most molecules also have paired electrons [9] giving a total electron spin $S = 0$ and a spin multiplicity of $2S+1 = 1$. These molecules are said to be in a *singlet state*, commonly referred to as S_0, S_1, S_2,... with increasing energy. For a molecule having an S_0 ground state, the excitation of an electron from a paired electron pair can produce a state where the two electrons still have opposite spins, for instance S_1, or a state where the two electrons are unpaired; they have the same spin direction. In the latter case the molecule's total spin equals one, giving a spin multiplicity of three. The molecule is now said to be in a *triplet state*, referred to as T_0, T_1, T_2,...

One exception from the usual molecular ground state of S_0 occurs in O_2. The common form of this molecule has a triplet ground state, $^3O_2$, which has been shown to react strongly with a photosensitizer (e.g. protoporphyrin IX) in its triplet form [11] — an interaction giving rise to singlet oxygen and the return of the photosensitizer to its ground state. This mechanism is demonstrated in Figure 2.1, where the excitation of $^3O_2$ into singlet oxygen is depicted as a consequence of the simultaneous deexcitation of a sensitizer's triplet state.

2.2 Wavelength dependence in PDT

The light used to activate the photosensitizer must be able to penetrate tissue to some amount if it is to reach not only superficial cells. The penetration depth increases with increasing wavelength, and there is some variability with tissue type, as can be seen in Table 2.1 [8, 12]. It is therefore important that the photosensitizer absorbs light with a relatively long wavelength, but not *too* long, as we need enough energy to produce singlet oxygen (ΔE = 94 kJ/mol [13] (= 5.9 eV/mol)). The wavelenghts between 600-850 nm can penetrate skin to some amount, and still be able to provide enough energy to excite oxygen from its triplet to its singlet state [13–15]. This means that the photosensitizer should absorb light within this interval to be relevant for use in cases where it is necessary for the light to penetrate skin/tissue. The absorption spectrum for PpIX in Figure 2.4 shows that it has an absorption peak at 635 nm as mentioned before, but it also shows that the absorption is many times less efficient than the absorption at 405 nm in the blue region[1].

2.3 Production of reactive oxygen species

Generation of reactive oxygen species may occur by a large number of physiological and nonphysiological processes, including their generation as by-products of normal cellular

[1]Both spectra are measured by the author and fellow student Magnus Berg Johnsen in the course TFY4 Optical Spectroscopy.

Table 2.1: Typical optical penetration depths, δ, in human tissue (left). Specific (measured) optical penetration depths in human tissues (right). δ refers to the depth at which the intensity of the light is 37% of its original value.

Wavelengths [nm]	δ **[mm]**
400 - 450	0.1 - 0.3
450 - 500	0.3 - 0.5
500 - 550	0.5 - 0.6
550 - 600	0.6 - 2
600 - 750	2 - 3
750 - 1200	3 - 5

Human tissue type	δ **[mm] at 633 nm**
Brain	0.8
Liver	0.9
Lung tumor	1.6
Kidney	2.5
Malignant prostate	2.8
Bladder TCC	4.0

metabolism, primarily in the mitochondria. Normally the oxidative stress in cells is balanced by the presence of scavengers, preventing the damage coming from ROS from exceeding toxic levels.

On the other hand, when the cells are exposed to PDT treatment, the ROS level in the cells exceed the threshold level, and the amount of damage can lead to cell death, both apoptotic and necrotic [16].

When the photosensitizer (PS) has been excited from the ground state to the first excited singlet state, an electron can undergo spin inversion and populate the first excited triplet state at a lower energy. A triplet molecule does not easily react with a singlet molecule, but if meeting another triplet molecule the magnetic fields created by the unpaired electrons can interact. The two molecules then exchange energy and become singlet molecules [10]. This is the origin of a type II photoreaction, one of the two reactions producing reactive oxygen species in photodynamic therapy.

Type I photochemical reaction: In this process free radicals (ex. $OH^{\bullet}$), peroxides (ex H_2O_2) and superoxides ($O_2{}^-$) are generated by electron or hydrogen transfer reactions from the PS to water or biomolecules, producing a cytotoxic result. The sensitizer reacts in this process directly with cell components and is chemically altered.

Type II photochemical reaction: The PS may also undergo an energy transfer with $^3O_2$, leading to deexcitation of the PS and excitation of the oxygen molecule to $^1O_2$, a very reactive form of oxygen which can oxidatively damage biomolecules. In this process, the sensitizer acts merely as a mediator.

In a type I photoreaction the photosensitizer can return to its ground state S_0 from another singlet state, while in a type II reaction the transition is from the T_1 to the S_0 state. Also, in the latter reaction the photosensitizer is not modified, but returns to its ground state without chemical alterations. In this way the process of energy transfer from the photosensitizer to oxygen can be repeated many times. It is generally accepted that the type II mechanism dominates in PDT, but both type I and type II reactions occur simultaneously. The ratio between the probabilities for the processes to occur

depends on the type of sensitizer used, the concentrations of substrate and oxygen, as well as the binding affinity of the sensitizer for the substrate [1, 15].

The generated singlet oxygen has a very limited lifetime($\leq$50 ns [17]) and diffusion length in biological tissue ($\leq$20 nm [15, 16]), meaning that the cellular targets are those in the immediate vicinity of the singlet oxygen production site. $^1O_2$ can react with a large variety of molecules, such as proteins, nuclear acids and lipids.

Singlet oxygen can also react with the PS, causing *photobleaching* by oxidation of the PS and thereby chemical degradation. If the PS is degraded it cannot contribute to further excitation of oxygen. During illumination, the amount of PS will therefore decrease, which could lower the efficiency of the photodynamic treatment. This may be one reason to try *fractionated* PDT, thus allowing the concentration of PpIX and oxygen to rise between consequent illuminations.

2.4 Mechanisms of cell death

Destruction of cells and tissue after PDT has been suggested to follow three principal mechanisms; cellular targeting, vascular damage or immunological response. In this project we are mostly interested in the cellular targeting — how dose, localization of the photosensitizer and the therapeutic conditions (such as the light delivery) influence the response of the cell. But *in vivo* these responses may be modified by the other two mechanisms. Vascular injuries induced by PDT can lead to tumor destruction by hypoxia and nutrient deprivation, and an inflammatory response to treatment could contribute to tumor destruction [9].

2.4.1 Terminology

It is common to distinguish between two types of cell death; apoptotic and necrotic. Apoptotic cell death is referred to as an active process following distinct steps, while necrotic cell death is described as passive, catabolic and degenerative — generally a response to gross injuries. Necrosis is often triggered by the same insults which at a lower intensity would cause apoptosis. It has been speculated that having two modes of cell death separated by a threshold damage may be a way to alert the organism of the extent of the damage and that this defines whether a repair response is required to maintain organismal integrity [18].

Some argue that one should, at least, include a third term when discussing cell death, *oncosis*, and reserve necrosis for changes secondary to cell death by any mechanism after membrane disruption [19–21]. Oncosis was proposed by Majno and Joris (1995) [19] to define the early stage of primary necrosis during which the cells swell. Other characteristics are swelling of organelles and increased membrane permeability. This is depicted in Figure 2.2.

Apoptosis is favoured over necrosis by clinicians as the risk of inflammation is lower and because cell death by apoptosis could have a multiplicative effect, improving the efficacy of the treatment. Thus, quantifying the apoptotic and necrotic fractions after PDT in different tumor cell lines is an important part of optimizing treatment protocol.

Apoptotic death

Apoptosis is a normal part of development and also a normal part of maintenance and defense of the adult human body. Actually, in our bodies, which consist of nearly 10^{14} cells, it is estimated that 10^{11} cells are eliminated each day through apoptosis [22].

Apoptosis is characterised by morphological and biochemical changes, followed by engulfment of cellular remains by phagocytosis [13]. The cell commits suicide in response to physiological signals and intracellular damage.

Two major apoptotic pathways have been characterized: the *death receptor-mediated* pathway and the *mitochondria-mediated* pathway. Both pathways lead to the activation of different caspases[2], which will change the cell's normal behaviour and lead to apoptotic death. In the first pathway, cell surface receptors from the tumor necrosis factor gene family are stimulated, leading to activation of caspase-8. In the second pathway, disruption of mitochondrial function, causing the release of cytochrome C to the cytosol, will induce processes leading to the activation of caspase-9 [23, 24].

In early stages of apoptotis the cell shrinks. Gradually the mitochondrial structure is changed and the chromatin is condensed followed by nuclear disintegration and formation of apoptotic bodies; the cell disintegrates into several vesicles. The fragments can then be engulfed by macrophages or other neighbouring cells. Other changes include loss of the mitochondrial transmembrane potential, activation of caspases and DNA fragmentation [22].

A key event is the translocation of one of the phospholipids situated in the plasma membrane, namely *phosphatidylserine*. Normally this phospholipide faces the inside of the cell, but in the early stages of apoptosis it is translocated to the opposite layer of the plasma membrane, facing the extracellular space. This is believed to be an "eat me" signal recognizable to other cells. The apoptotic fragments will then be phagocytized by other cells or macrophages [25].

Necrotic death

Necrosis is believed to be a less ordered form of cell death following events like infection, physical injury, ischemia, or excessive accumulation of ROS. The early stages of necrosis are characterized by swelling followed by rupture of the plasma membrane and subsequent release of cytoplasmic constituents. This may also be harmful to neighbouring cells, and necrosis often triggers an inflammatory response when arising in living organisms [18, 22].

2.4.2 How does ROS-generated injuries lead to cell death?

The cell's main membrane components are lipids and proteins, and the cell's functionality is based on enzymes and proteins behaving in a correct manner. As reactive oxygen species can modify both lipids and proteins, they represent a threat to the cell when they appear in large amounts.

Proteins and lipids can suffer injuries from ROS-attacks on double bonds in polyunsaturated fatty acids, amino acid residues with sulfur or proteins with sulfhydral links.

[2]Caspases: Cysteine aspartic acid proteases.

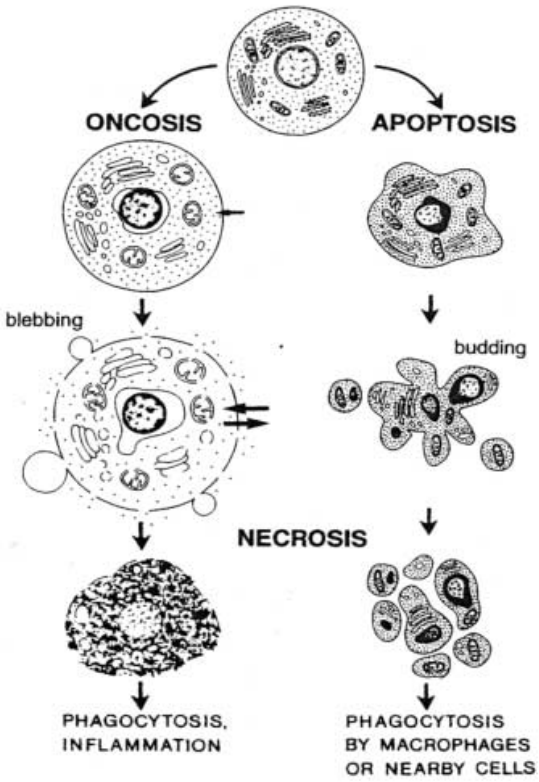

Figure 2.2: An illustration of how both apoptosis and oncosis can lead to a final stage of necrosis. In cell culture, the apoptotic bodies are not engulfed by macrophages and will enter apoptotic necrosis with membrane rupture [19].

Modifications of amino acids can change functions of proteins such as enzymatic activity, which unrepaired can lead to dysfunction and cell death.

Lipid attacks can lead to necrosis through loss of membrane integrity of both the plasma membrane and internal membranes such as the lysosomal membrane. Necrosis can also follow an intracellular leak of proteases from the lysosomes or an uncontrolled influx of extracellular Ca^{2+} [18].

Apoptosis is initiated by biochemical signals. Many of these converge in the mitochondria activating the mitochondrial-mediated pathway. The intermembrane space of these organelles contains several proteins which can initiate the apoptotic pathway when released through pores in the inner or outer mitochondrial membrane. This process is again controlled by other proteins [23]. It is proposed that PDT can lead to apoptosis by direct induction of mitochondrial pore opening [23], and it has been found that apoptosis also follows oxidative stress imposed on endoplasmic reticulum (ER), contributing to the cytotoxic effect of ALA-PDT [26].

Oxidative damages to proteins, lipids or DNA may all have a toxic effect on cells. However, proteins are often catalysts rather than stoichiometric mediators, and damaging one protein would give an effect greater than a stoichiometric one [27]. Recent studies also show that the oxidation of proteins could be selective [28–30] and may play

a role in the signaling events which lead to apoptosis or necrosis in cells.

2.5 PDT based on aminolevulinic acid or its esters

A crucial step in PDT is the production of singlet oxygen, commonly written as $^1O_2$, or other reactive oxygen species. The photosensitizer acts as a mediator between the incoming light and the potential ROS. Singlet oxygen seems to be accepted as the most important reactive oxygen species to produce photodynamical injury in biological systems [4, 15], but the other ROS are also capable of inducing cell death.

To which extent ROS are formed, and where, depends on the choice of photosensitizer. In this project HAL (hexyl-ALA) induced *protoporphyrin IX* (PpIX) was used.

The history of ALA-PDT started in 1987, when Malik and Lugaci used ALA induced PpIX with light to inactivate cells in vitro, and Peng *et al.* at the same time performed *in vivo* experiments. It is now a widely practised form of PDT [2], as is evident from the list of currently opproved clinical photosensitizers, shown in Table 1.1.

2.5.1 The photosensitizer

PpIX is an intermediate in the *heme*[3] biosynthesis which takes place in all nucleated cells. It can be induced by the heme precursor *5-aminolevulinic acid* (5-ALA) or one of its ester derivatives. Heme is not a photosensitizer in itself, because of the centrally inserted paramagnetic Fe^{2+} ion, which causes a significant reduction in excited state lifetimes [13]. Neither is 5-ALA or its esther derivatives. (See Figure 2.3.)

PpIX is a member of a class of molecules called macrocycles, a family containing many porphyrins. These are highly conjugated molecules that have a large π-electron-rich fused ring with considerable delocalization of the π-electrons[4]. Such molecules exhibit several π-$\pi*$ transitions, because of the prensence of many π and $\pi*$ molecular orbitals. Porphyrins in general absorb most efficiently at approximatly 400 nm (the Soret band), but exhibit a series of weaker π-$\pi*$ transitions in the 450-650 nm interval, called *Q-bands* [9]. While the Soret band arises from a strong electronic transition from the ground state to the second excited singlet state ($S_0 \rightarrow S_2$), the Q-band is a result of a weak transition to the first excited singlet state ($S_0 \rightarrow S_1$) [13]. Different π-$\pi*$ transition possibilities give rise to the specific absorption spectra of each porphyrin and are influenced by the surroundings. PpIX has a π-$\pi*$ transition corresponding to absorption of light with a wavelength of 635 nm (in ethanol) which is suitable for PDT. The absorption spectrum for PpIX is shown in Figure 2.4. PpIX will, as shown in the same figure, also exhibit fluorescence, which can be used for evaluating its intracellular localization for instance by using a confocal laser microscope.

[3] Heme is a functional (conjugated) group of e.g. hemoglobin, which binds and releases oxygen [9], but also several other proteins carry this group.

[4] π-electrons occupy molecular orbials called π-orbitals, binding orbitals in molecules. $\pi*$-orbitals are anti-binding molecular orbitals, with a higher energy than π-orbitals.

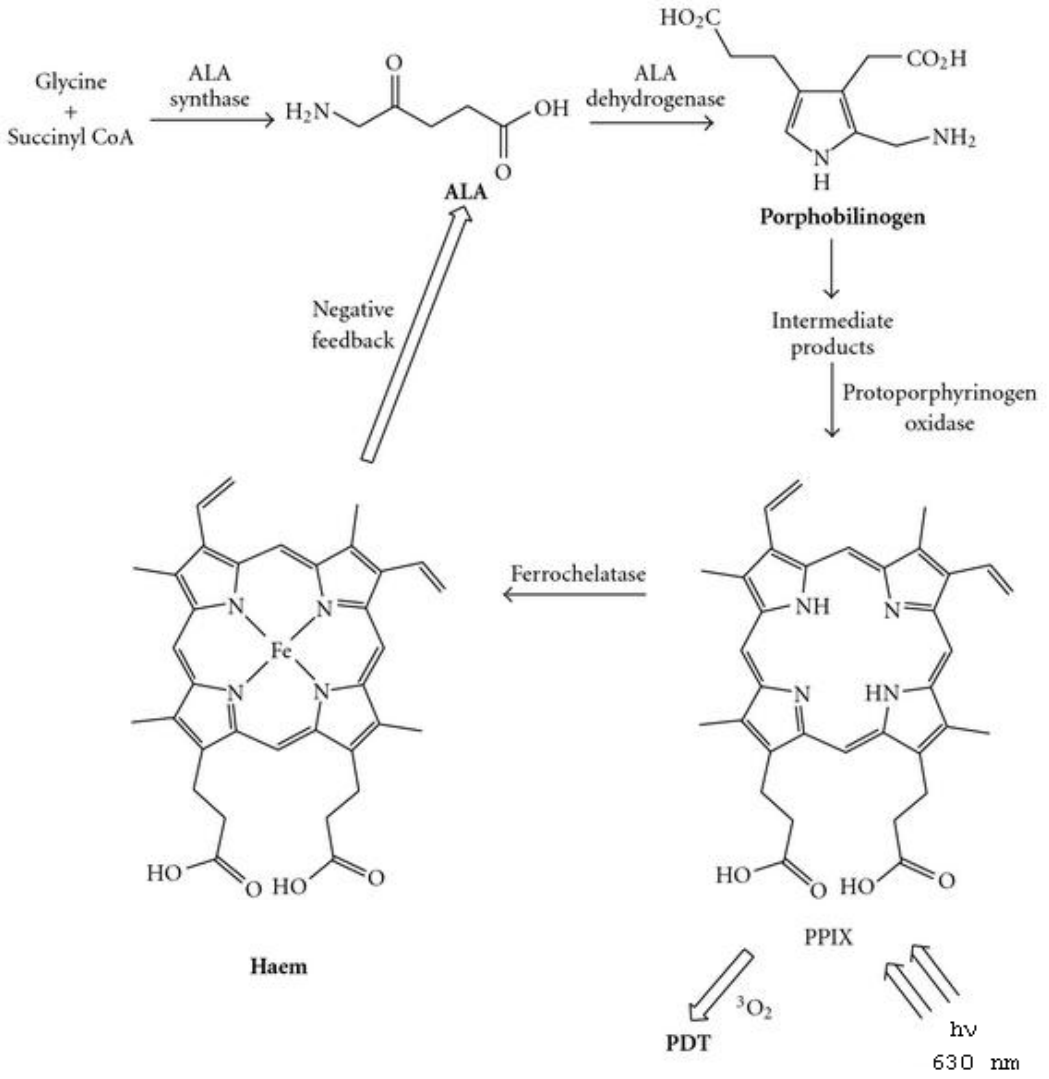

Figure 2.3: Simplified heme biosynthesis. Adapted from [13]

2.5.2 Endogenous production of PpIX

Heme is synthesised in all energy producing cells in the body, and PpIX is, as mentioned before, the immediate precursor of heme (Figure 2.3). As shown in Figure 2.5, cellular production of PpIX is located both in the mitochondria and in the cytosol. In mammals and photosyntetic bacteria the precursor 5-ALA is formed from the easily available compounds glycine and succinyl-CoA [4], a process catalysed by *5-aminolevulinic acid synthase* (ALAS).

ALAS is one of eight enzymes in the heme biosynthetic pathway, and has a main regulatory function, which also include inhibition by heme. This is an example of negative feedback regulation. The regulation will be bypassed when 5-ALA is introduced in

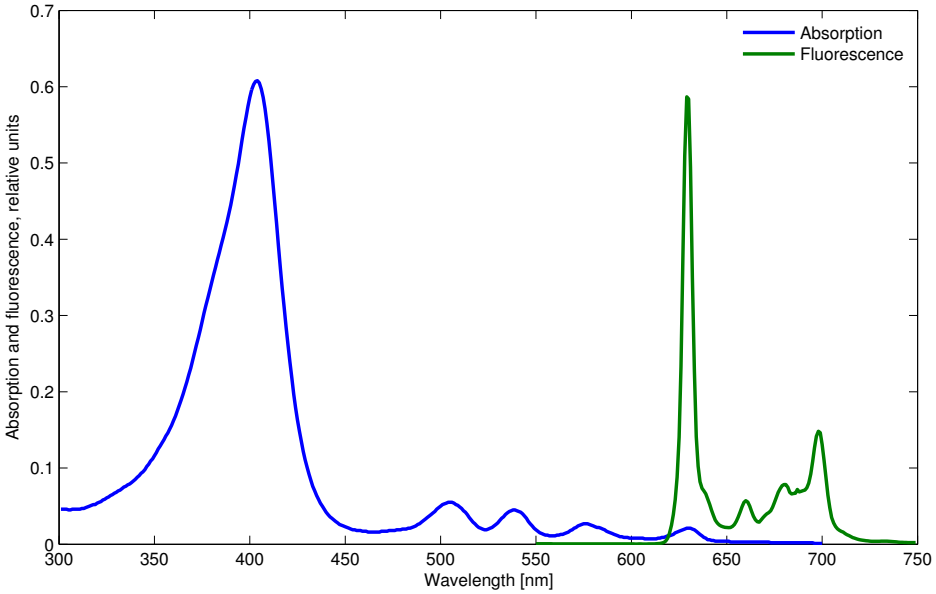

Figure 2.4: Absorption spectrum of PpIX in ethanol shown in blue. Fluorescence emission spectrum of PpIX in ethanol shown in green. Notice that only fluorescence resulting from a depopulation of the S_1 state to different vibrational levels of the S_0 state is observed. This is because the dissipation of energy via internal conversion from the second excited singlet state is an extremely rapid process, so efficient that fluorescence is never observed from the S_2 to the S_0 state [31].

excess, leading to an accumulation of PpIX. The accumulation is larger in cancer cells than in normal cells. The reason for this increased accumulation is not fully understood, but changes in the activity of enzymes catalyzing the different steps in the synthesis can be relevant.

One example is the activity of *ferrochelatase*, which has been shown to have a lowered activity in some pre-malignant and malignant tissues. This enzyme is responsible for the last step in the heme biosynthesis; inserting an iron atom in PpIX. Lowered activity of this enzyme could then explain some accumulation of PpIX in cancer cells [32]. Other enzymes catalyzing the production of intermediates have been shown to have an increased activity in malignant tissues, leading to a more efficient production of PpIX [33]. The vascularity and pH of cancerous tissue is different from healthy tissue and can lead to a difference in photosensitizer uptake, which can also be caused by the poor lymphatic drainage in such tissues [1, 3, 15].

Cellular uptake of the precursor

If PpIX is to be produced from ALA, not only must ALA cross the cell's plasma membrane but also surrounding tissue. This molecule is hydrophilic, and does not cross cell membranes (or tissue) easily. There are however many other advantages of using ALA

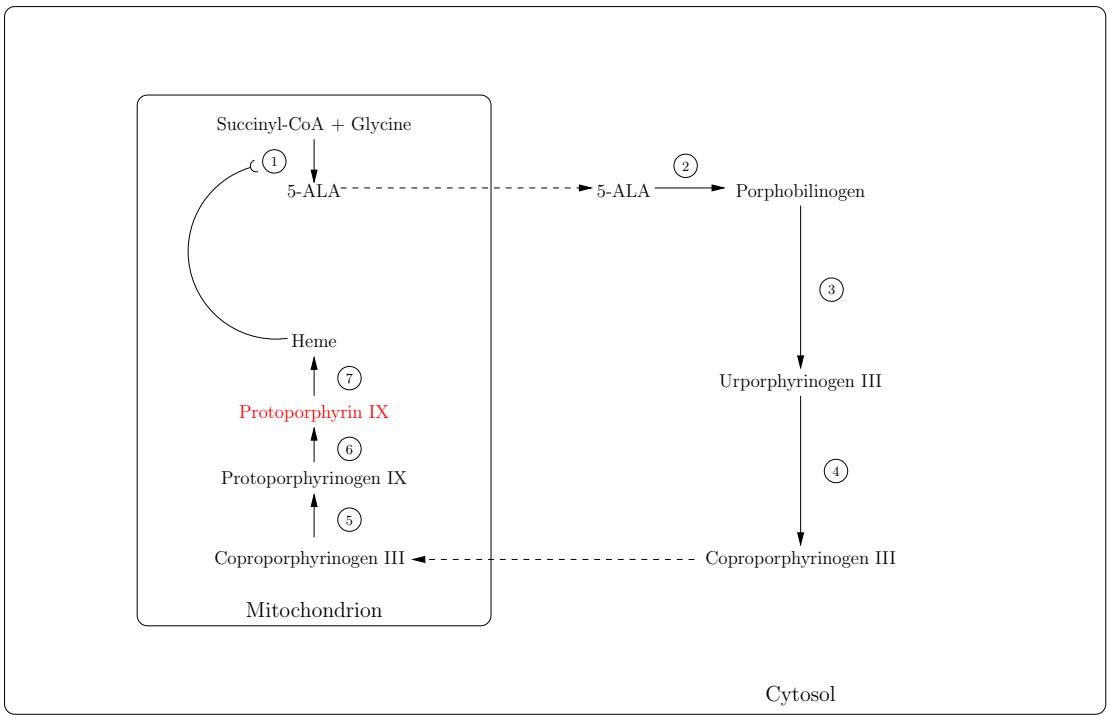

Figure 2.5: A schematic depiction of the endogenous production of PpIX in eukaryots. The production cycle takes place both in the cytosol and in the mitochondria. Numbers denote different enzymes catalysing the processes. Enzymes mentioned in this text are number one, *ALAS*, which is inhibited by heme, and number seven, *ferrochelatase*, which catalyses the insertion of Fe^{2+} into PpIX in the formation of heme.

as a precursor. One is the possibility of monitoring sensitizer levels *in situ* by means of fluorescence. Another advantage is the rapid systemic clearance of the photosensitizer (24-48 h). And of course, ALA is a "bio-compatible" molecule. This is a clear advantage over other chemically synthesised photosensitizers, which do not exist naturally in cells.

In this project, the lipophilic ester derivative hexyl-ALA (HAL) has been used as a precursor to ease the cell membrane crossing. The uptake of ALA is an active process, while HAL crosses the plasma membrane through passive diffusion. In addition, esters such as HAL has been shown to accumulate faster and induce more porphyrins than ALA itself (references from [4, 17, 34]). HAL is also approved by the European Union for photodetection of bladder cancer (Table 1.1), and is therefore a promising compound for PDT therapy.

HAL is converted by esterases in the cells into ALA, which then is used in the production of PpIX. The localization pattern of PpIX has been shown to be similar when using ALA or HAL as a precursor [35].

2.6 Photosensitizer localization and the effects on cell death

Because of the very limited diffusion length of singlet oxygen in tissue, the localization of the photosensitizer is very influential to the induction of cell death. PpIX is a lipophilic molecule, and it has been shown that endogenously produced PpIX in AY-27 cells treated with HAL localize in membrane structures throughout the entire cell. Thus the photosensitizer can induce injuries at various sites in the cell, including the cell's plasma membrane, the ER, lysosomes or mitochondria [35]. According to Plaetzer *et al.*, PDT induced damage to these organelles can all lead to active cell death (apoptosis) [23].

In contrast to ionizing radiation, PDT is not likely to have any significant carcinogenic effect on surviving tissue. This conclusion is based on the fact that practically none of the photosensitizers tested for PDT enter the nucleus, and therefore they have a low potential for producing mutations [36].

As PpIX is formed in the mitochondria of eukaryotic cells, one would expect mitochondria to be important targets of ALA-PDT. Mitochondria have indeed been shown to be initial targets after this treatment [17]. Since targeting of mitochondrial functions is a mechanism for inducing apoptosis [37], some of the cytotoxicity of PDT could be associated with triggering the mitochondrial apoptotic pathway. As mentioned earlier, evidence of apoptosis following the mitochondrial pathway has been found [23, 26].

It has been shown that PDT is effective even in cancer cells *resistant* to apoptosis [18], and it is believed that necrosis is the dominant path at least for large PDT doses [36], while apoptosis is more important at smaller doses. The fact that PDT is effective even in cells otherwise resistant to apoptosis can imply that necrosis is the more important pathway, but also that apoptosis is triggered at a late stage after PDT, bypassing the normal signaling process initiating the mitochondrial apoptotic pathway.

2.7 Fractioning the light delivery

In radiotherapy[5], it has been found that fractionation of the radiation dose will produce, in most cases, better tumor control for a given level of normal-tissue toxicity than a single large dose [38]. Fractionation exploits the difference between sublethal damage repair in normal tissue and tumors, and will also allow tumor reoxygenation between doses, which increases the radiosensitivity of the tumor.

There are similarities beween survival curves obtained by PDT and ionizing radiation, such as a shoulder region for low doses. Repair of sublethal PDT damage has been documented in some split-dose experiments [39], but it is not known whether or not a repair differential exists between normal and diseased tissue.

As oxygen is needed to produce a cytotoxic effect in PDT, reoxygenation during dark intervals could increase the effect of photodynamic treatment if depletion of oxygen is a problem. The amount of available photosensitizer is also a rate limiting factor in PDT, and in HAL-PDT the formation of new PpIX molecules from HAL in the tissue/cells during a short dark period could result in an increased therapeutic effect.

[5]The treatment of disease with ionizing radiation.

2.8 Theoretical survival curves — hit theory

Dose response curves obtained in PDT experiments can be interpreted using hit theory, originally developed for survival curves after treatment with ionizing radiation. Although the model has limitations, parameter values obtained by using this theory provides information which can be used in comparison of different treatments or treatment regimes.

The model is based on two physical observations and one postulate [40]. Translated to the case of PDT, they become:

1. Light transfers energy in discrete packages (photons).
2. The interactions (hits) are independent of each other and follow a Poisson distribution.
3. The response under investigation occurs if a specified target has recieved a defined number of hits.

If the radiation sensitivity is ν, and the dose is D, the Poisson distribution gives the probability of recieving exactly m hits, as

$$P(m) = \frac{(\nu D)^m}{m!} e^{-\nu D}.$$

If the object of interest has n targets, each needing m hits for inactivation, then the probability of survival S, is

$$P(S) = 1 - \left(1 - e^{-\nu D} \sum_{m=0}^{m-1} \frac{(\nu D)^m}{m!}\right)^n. \tag{2.1}$$

A special case of equation (2.1) is the single hit, multi target model, which has been used to describe survival curves following photodynamic treatment (e.g. [41]). In this case, each of the n targets need exactly one hit for the object to be inactivated. This model seems appropriate if the object to be inactivated is a cell, containing many potential protein and lipid targets. If the number of inactivated biomolecules is large enough, the cell wil not be able to maintain its normal functions, and it will die.

If the radiation sensitivity is given by $\nu = 1/D_0$, the expression for the survival in the single hit, multi target model becomes

$$P(S) = 1 - (1 - e^{-D/D_0})^n. \tag{2.2}$$

Chapter 3

Experimental methods

3.1 Motivation for this chapter

To perform your experiment correctly, it is important to understand the techniques you are using. Knowing the limitations of the instruments or reagents used is important to be able to process and discuss the results obtained. A chapter briefly covering each method used in the project is therefore included, but the methods are described in further detail in chapters 4 (p. 25) and 5 (p. 49).

3.2 The MTT assay — measuring mitochondrial activity

If you are not concerned about the *type* of cell death achieved after PDT, survival of the treated cells can be measured by the *MTT assay*. One alternative to this method is colony counting, but the MTT assay is the method commonly used with PDT on AY-27 cells, and is quite easy to perform. It is common to do the analysis 24 h after treatment, and e.g. the LD_{50} dose can be determined from the information obtained. This dose is often of interest when planning other experiments where for instance the total protein content after treatment is important for further studies. In this study it was used as an alternative method in measuring the effect of fractionated therapy.

Yellow MTT, a tetrazolium salt, is reduced to purple *formazan* in the mitochondria of living cells (Figure 3.1). These reductions take place only when mitochondrial reductase enzymes are active, that is when the mitochondria is not dysfunctional.

The reduction product, formazan, is water insoluble. Isopropanol can be used to dissolve the purple formazan precipitate into a colored solution, and the absorption can be measured with a spectrophotometer. The absorption peak will depend on the solvent used. When isopropanol is used, the absorption is measured at $\lambda = 595$ nm.

When the amount of formazan produced by cells having recieved PDT is compared with the amount of formazan produced by untreated cells, the effectiveness of the PDT treatment can be deduced. There will be a linear relationship between the number of living cells (cells with intact mitochondrial reductases) and the absorbance of the colored solution [42]. This way the absorbance can be used to measure the relative amount of living cells after PDT treatment.

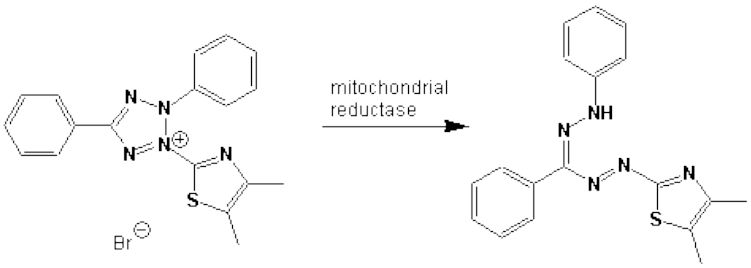

Figure 3.1: Illustration of the reduction of MTT to formazan by the enzyme mitochondrial reductase.

3.3 Distinguishing between apoptotic and necrotic cells

It is of great interest to know how and when the cells die after treatment. One way of sorting the cells in the categories viable, apoptotic and necrotic are by fluorochrome staining followed by flow cytometry or confocal laser scanning microscopy (CLSM).

3.3.1 Fluorochrome tagging by Annexin V Fluos and Propidium Iodide

Two dyes (fluorochromes) are commonly used to differentiate between apoptotic and necrotic cells in a population, *Annexin V Fluos* (Ax) and *Propidium Iodide* (PI). The labelling and detection of apoptotic cells is based on changes in the outer leaflet of the plasma membrane. In viable cells, the phospholipide *Phosphatidyl serine* (PS) is directed towards the cytoplasm. However, in apoptotic cells, PS appears on the outer leaflet towards the extracellular environment, where it can bind to fluorescent Annexin V-conjugates [23].

Cells with highly permeable or broken plasma membranes, necrotic cells, will display fluorescence from PI, as PI binds to double stranded nuclear acids; DNA or RNA. Necrotic cells will also display fluorescence from Ax, as it can bind to PS in the inner leaflet of the plasma membrane.

Early apoptotic cells are impermeable to PI, but will display PS on the outer leaflet early in apoptosis. This event preceedes cell membrane permeabilization, cell shrinkage and nuclear condensation, and is used as a marker of early apoptosis [43].

Combined, Ax and PI is used to separate the cell population in three; viable, apoptotic and necrotic cells. The fluorescence can be detected e.g. in a flow cytometer or a confocal microscope. The absorption and emission spectra of PI and Ax are given in Figure 3.2a.

3.3.2 Fluorochrome tagging by YO-PRO-1 and Propidium Iodide

As mentioned earlier, the permeability of the cell membrane changes during apoptosis. Assays for apoptosis using YO-PRO-1[1] and PI use these permeability changes to differentiate between viable, apoptotic and necrotic cells. Viable cells are not appreciably

[1]See Abbreviations ,page ix.

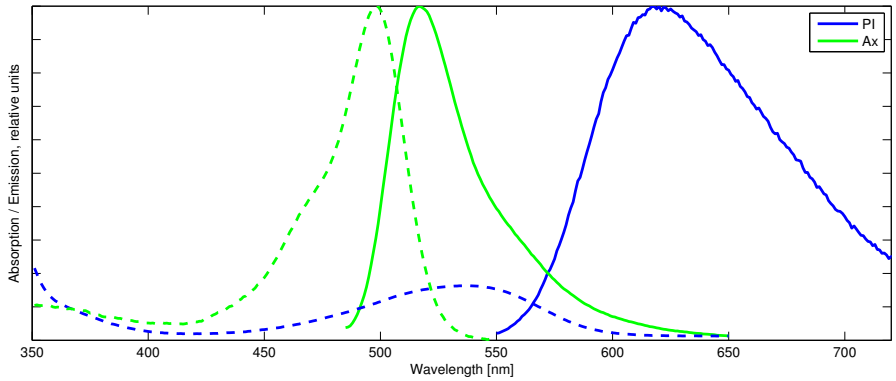

(a) Ax/PI

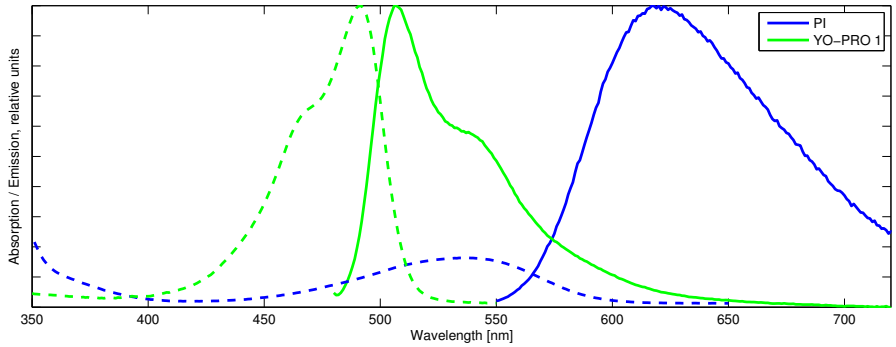

(b) YO-PRO-1/PI

Figure 3.2: The absorption (dashed line) and fluorescence (solid line) spectrum of the fluorochromes used in this study. All fluorochromes were excited at 488 nm. (Source of data: Invitrogen)

stained by either YO-PRO-1 or PI, and YO-PRO-1 will enter the cell at an earlier stage in apoptosis than PI. Necrotic cells are permeable to both dyes.

The absorption and emission spectra of PI and YO-PRO-1 are given in Figure 3.2b.

3.4 Flow cytometry

Cells which are to undergo flow cytometry must be in suspension, as measurements are done in a single cell manner. To obtain quantitative measurements, cellular molecules must be labelled by fluorescent molecules in a stoichiometric manner. These fluorochromes are excited by a light pulse from a laser source, and the detected fluorescence is ideally proportional to the property in question. In this study, an argon laser line at 488 nm was used to excite the fluorochromes. Correct measurements are based on equal illumination of each cell. This is achieved through hydrodynamic focusing of the cell suspension and an elliptical illumination field.

In hydrodynamic focusing the cell suspension is enclosed in a sheath fluid producing a single particle flow. A schematic of the flow cell is shown in Figure 3.3. The velocity of the sheath fluid defines the particle velocity independently of individual size, which ensures equal illumination time for all particles.

Beam shaping optics is used in the laser beam path to make an elliptical focus spot in the laminar flow region of the flow cell of approximately 60 μm perpendicular to the fluid flow and 20 μm in the direction of the flow. The advantage of using an elliptical over a circular focus spot is that the elliptical focus provides a wider illumination field across the width of the flow so that the optical response does not fluctuate if cells stray from the center of the beam. The short dimension parallel to the flow ensures that only one cell hits the focal volume at one time [9, 44].

Fluorescent light is detected by several photomultiplier tubes (PMTs) according to wavelength. In addition to fluorescence, scattered light is also detected. Low angle scattering resulting from diffraction of the beam is detected by a photo diode and give information about cell size. High angle scattering resulting from reflection and refraction on cell structures is detected by another PMT and give information about structure or granularity of the cells [9].

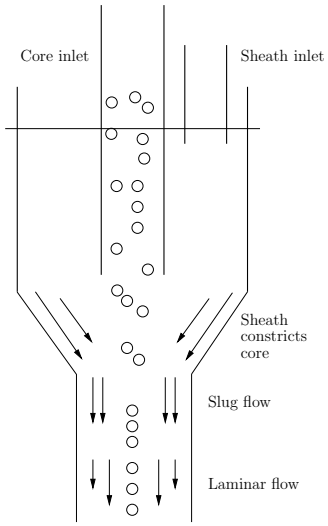

Figure 3.3: A schematic depiction of single cell flow obtained by hydrodynamic focusing in the flow cell.

3.5 Confocal laser scanning microscopy

In a conventional wide-field microscope, thick specimens will produce an image that represents the sum of sharp image details from the in-focus region, combined with blurred images from all the out-of-focus regions. This problem is overcome in confocal microscopy by introducing a variable pinhole in the path of the image forming beam (e.g. fluorescence) as shown in Figure 3.4. The pinhole rejects the out of focus contribution because light from other object planes than the focal plane do not converge at the pinhole and is blocked. In addition the pinhole blocks much of the stray light in the optical system.

To build a 2D image the focused laser beam is scanned in a raster pattern over points in an xy-plane of the specimen. A 3D image can be reconstructed from such optical sections by scanning the specimen with different heights of the focal plane [9, 44].

In this study, an Argon laser line at 488 nm was used to excite the fluorochromes. The fluorescent light was detected in the range of 500 nm - 550 nm (Ax), and 650 nm - 720 nm (PI), which excludes the excitation beam.

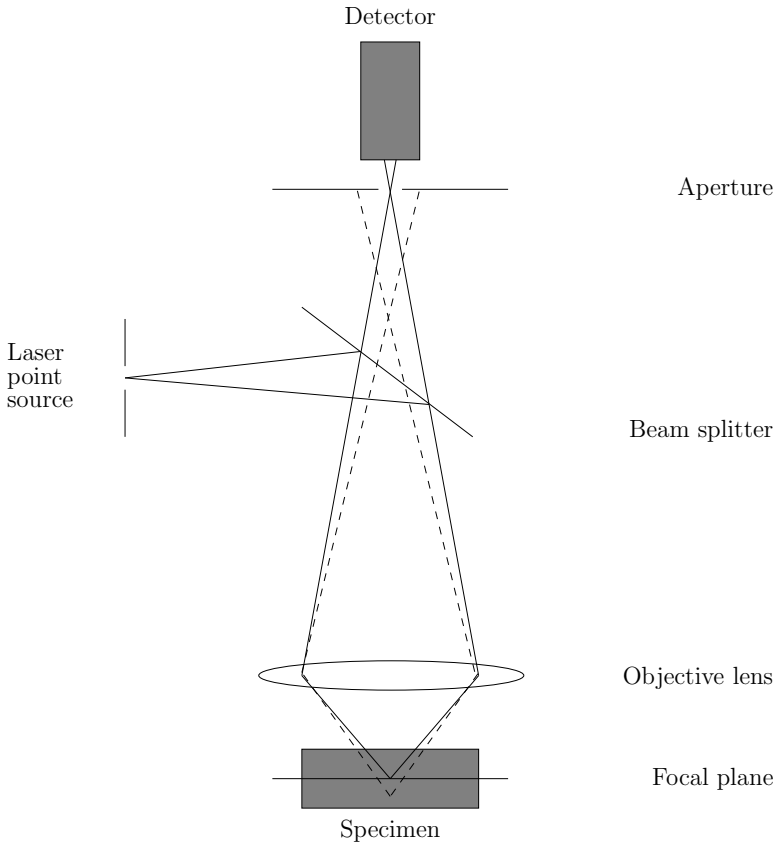

Figure 3.4: Schematic figure showing the principle of confocal imaging, where an aperture (a pinhole) is used to block light not originating from the focal plane.

Chapter 4

Materials and methods

4.1 Culturing the cell line AY-27

AY-27 cells originate from rat bladder transitional cell carcinoma (TCC), and grow in a monolayer [45]. An ideal number of $2 \cdot 10^6$ cells were seeded in 75 cm^2 cultivation flasks twice a week in 15 ml cultivation medium. The cultivation medium consisted of RPMI-1640 supplemented with *fetal bovine serum* (FBS) and L-glutamine. 50 ml FBS and 1.7 ml L-glutamine was added to 500 ml RPMI-1640. The cells were incubated in a Binder incubator at a temperature of 37 °Cwith a humified atmosphere containing 5% CO_2.

Cultivation medium, PBS, FBS, accutase and MTT were all purchased from Sigma-Aldrich, while Petri dishes and well plates were obtained from Nunc. HAL was kindly provided by Photocure ASA (Oslo).

4.2 The light source

The light source used in the experiments was an Aktilite lamp, model CL-128 from Photocure ASA. The lamp was situated in a room holding a temperature of 37°C. To lower the irradiance and to make the light more homogenous, a housing with a diffuser plate (white glass) on top was used. In this setup, the irradiance was measured to be on average 20 mW/cm^2 on top of the diffuser.

The spectrum of the lamp had previously been measured, showing a peak at 631 nm, which was used in calculations regarding the dose recieved by the cells, see Figure 4.1.

4.2.1 Light absorption measurements

To quantify the irradiance of the light hitting the petri dishes or wells and the dose given to the cells during irradiation, irradiance measurements were performed on the light source using a PAR[1] detector (LI-COR Quantum Detector, type LI-190SA).

Inspired by the *in vivo* experiments performed by Larsen *et.al* [7], it was decided to use an irradiance of 20 mW/cm^2 in this study.

[1] Photosynthetically Active Radiation

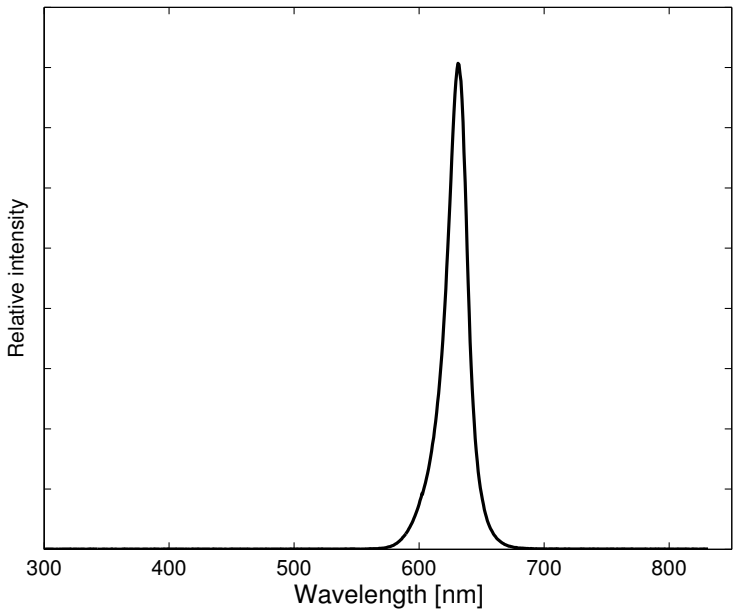

Figure 4.1: Spectrum of the red light source used in the PDT experiments [12].

4.3 Pilot studies

One of the objectives of this study was to compare flow cytometry techniques to confocal microscopy techniques when quantifying apoptosis and necrosis after PDT experiments. In the pilot studies, we tried to make protocols suitable for comparison of results between the two modes of measurement, which hopefully would lead to more reliable results. Protocols tested in the pilot studies are included in the following pages.

4.3.1 Use of Annexin V Fluos and Propidium Iodide

A common way of detecting apoptosis and necrosis is using the nuclear dye Propidium Iodide (PI) and Annexin V Fluos (Annexin, Ax). The selectivity is based on the flipping of phosphatidylserine in the plasma membrane of the cell early in apoptosis. As viable cells are impermeable to PI and Ax, necrotic cells are permeable to both, and apoptotic cells will bind Ax on the outside of their plasma membrane, this method separates the population in three.

Annexin binds to PS in a calcium dependent manner, and an incubation buffer was used to obtain the correct concentrations of ions. Contents of the Hepes buffer (pH 7.4) is given in Table A.2.

In addition to the modes of cell death after HAL-PDT, the effect of using Accutase in detachment of cells instead of Trypsin/EDTA was to be observed. All results can be found in the next chapter.

Obtaining comparable results with flow cytometry and confocal microscopy

As a first attempt, the experimental design as shown in Figure 4.2 was used. This design gives equal treatment and stress level to all samples before detection in a flow cytometer or confocal microscope.

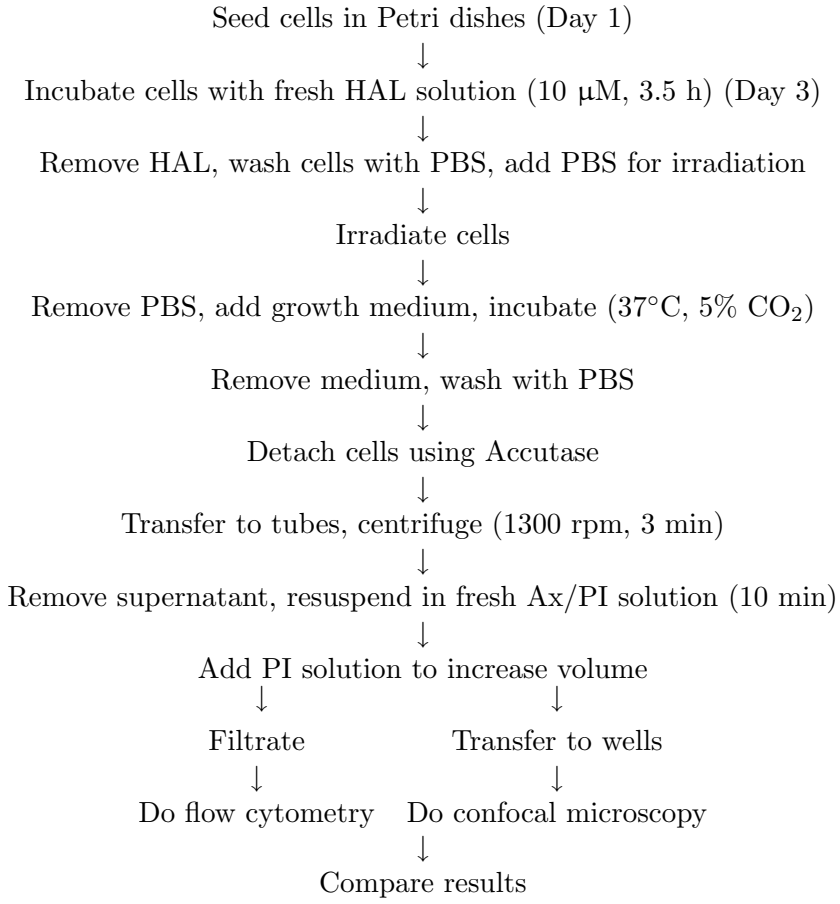

Figure 4.2: Protocol used in pilot studies of the apoptotic and necrotic fraction after HAL-PDT on AY-27 cells, using Ax and PI as fluorescent markers.

Optimization of each method of detection

A second option is to optimize the methods for either flow cytometry or confocal microscopy. The cells will then recieve minimal handling before observation, but the results from flow cytometry and confocal microscopy observations will differ to some extent, and may not be compared directly. Samples to undergo flow cytometry are handled as described in Figure 4.2, while samples to undergo confocal microscopy after treatment are handled as described in Figure 4.3.

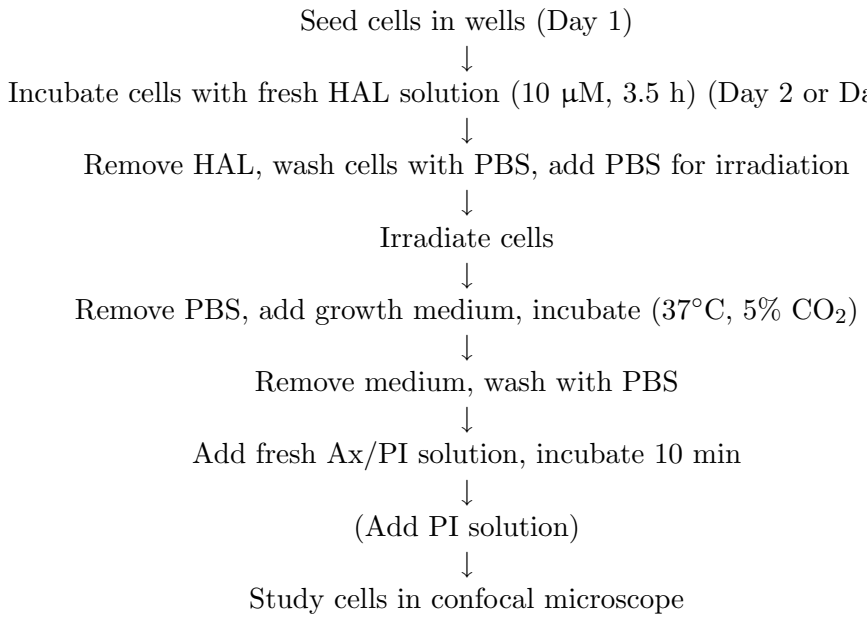

Figure 4.3: Protocol used in confocal microscopy studies of AY-27 cells after HAL-PDT treatment, using Ax and PI as fluorescent markers.

4.3.2 Use of YO-PRO-1 and Propidium Iodide

As earlier studies have reported some problems with the Ax/PI assay and because we measured a surprisingly low level of apoptosis in our experiments, we decided to try a combination of fluorochromes which did not rely on Annexin V binding to phosphatidylserine. If the results were drastically different, we would consider other methods for the detection of apoptosis in the AY-27 cell line.

It was decided to try change in membrane permeability as a marker of apoptosis, measuring fluorescence by flow cytometry and confocal microscopy with the nuclear stains YO-PRO-1 and PI. As the cell goes through apoptosis, the permeability of the cell membranes will change gradually. According to the manufacturer of *Vybrant Apoptosis Assay Kit 4* (Invitrogen), necrotic and apoptotic necrotic cells will be permeable to both nuclear stains, while early apoptotic cells are only permeable to YO-PRO-1. Viable cells will not be permeable to either of the fluorochromes.

Seed cells in Petri-dishes (Day 1)
↓
Incubate cells with fresh HAL solution (10 μM, 3.5 h) (Day 3)
↓
Remove HAL, wash cells with PBS, add PBS for irradiation
↓
Irradiate cells
↓
Remove PBS, add growth medium, incubate (37°C, 5% CO_2)
↓
Remove medium, wash with PBS
↓
Detach cells using Accutase
↓
Transfer to tubes, centrifuge (1300 rpm, 3 min)
↓
Proceed work on ice
↓
Resuspend cell pellet in cold PBS (1 ml) containing YO-PRO-1 (1 μl, Invitrogen) and PI (1 μl, Invitrogen)
↓
Incubate (25 min, on ice)
↓
Filtrate
↓
Do flow cytometry

Figure 4.4: Protocol used in flow cytometry studies of AY-27 cells after HAL-PDT treatment, using YO-PRO-1 and PI as fluorescent markers. The protocol had some minor changes, such as no detachment, when the cells were grown in well plates and examined by confocal microscopy.

4.4 Protocols used in the remaining studies

As can be seen in Chapter 5, difficulties with the confocal microscopy experiments made us choose flow cytometry in the remaining studies. Also, as there were no clear advantages found with the use of the alternative fluorochrome, Annexin V Fluos and propidium iodide were used to separate necrotic and apoptotic cells, as described in Figure 4.2. The incubation time post-PDT was either 1 hour or 24 hours.

4.4.1 Preparation of the cells and the photosensitizer

Two days prior to treatment with PDT, the cells were seeded in Petri dishes (r = 3 cm) at a concentration of $1.5 \cdot 10^4$ cells per ml cultivation medium, for a total of $6 \cdot 10^5$ cells ideally. On the day of the experiment, a stock solution of 10 mM HAL was made (2.52 mg HAL/ml pH 6.0 PBS) and sterile filtrated (0.22 μm). Cultivation medium without FBS was used to make a working solution (10 μM). Cultivation medium without fetal bovine serum was used because it has been found to influence the intracellular PpIX content, by extracting PpIX out of the cell.

4.4.2 Photodynamic therapy

The cells were washed in PBS, incubated with HAL (10 μM, 3.5 h) and washed in PBS again (x2). A minimum of two Petri dishes were used as control samples in the experiments, not recieving neither HAL nor light. Two Petri dishes recieved only the photosensitizer to reveal any toxicity and the rest were irradiated from 15 s to 30 min, depending on the experiment. The cells were irradiated with 2 ml PBS present. After irradiation, the PBS was removed from the Petri dishes and regular cultivation medium given. The cells were then incubated for 1 h or 24 h depending on the experiment, before viability or mode of cell death was examined by flow cytometry, confocal microscopy or the MTT assay.

Some remarks regarding the flow cytometry experiments

After the post-PDT incubation time, the cells were detached by adding 3.3 ml Accutase (20 min, 37 °C) to the dishes after washing with PBS. Further treatment was performed as described in Figure 4.2 with the instrumentsettings given in Appendix A.4.

The cells were collected with their supernatants if the post-PDT time was 24 hours, while they were collected without their supernatants if the post-PDT incubation time was only 1 hour. Results from pilot studies (data not included) showed that the total cell count in supernatants 1 hour after PDT was negligible compared to the cell counts from the detached cells, and that apoptotic cells were not overrepresented compared to the detached cell population. Thus by not including the supernatants in the 1 h samples, we did not lose any information. 24 hours after treatment, more cells have detached as they proceed through apoptotic or necrotic cell death, and the supernatants were collected before the cells were detached

Some remarks regarding the confocal microscopy experiments

In the experiments where confocal microscopy was used, incubation, irradiation and examination of the samples were done in several intervals, to avoid a queue of samples waiting to be examined. While flow cytometry of one sample is done in 1.5 minutes (20000 counts, 250 counts/s), focusing and capturing of one image in each of eight wells (one sample) may take more than five minutes.

The MTT assay

In the studies of fractionated light delivery, also the MTT assay was used to determine survival after treatment, and the protocol can be seen in Figure 4.5. A stock solution (5 mg/ml) was made, kept refrigerated (4 °C) and protected from light. At the day of the experiment, a working solution (0.5 mg/ml, 37 °C) was made using regular cultivation medium. The cells were incubated with the working solution for 1 hour, before isopropanol (2 ml) was added and the petri dishes placed on a shaker (500 rpm, 30 min). The colored solution was transferred to tubes and centrifuged (5 min, 1500 rpm). Absorption measurements of the supernatants were performed immediatly (λ = 300 nm - 700 nm) on a Shimadzu UV-160 1PC spectrophotometer.

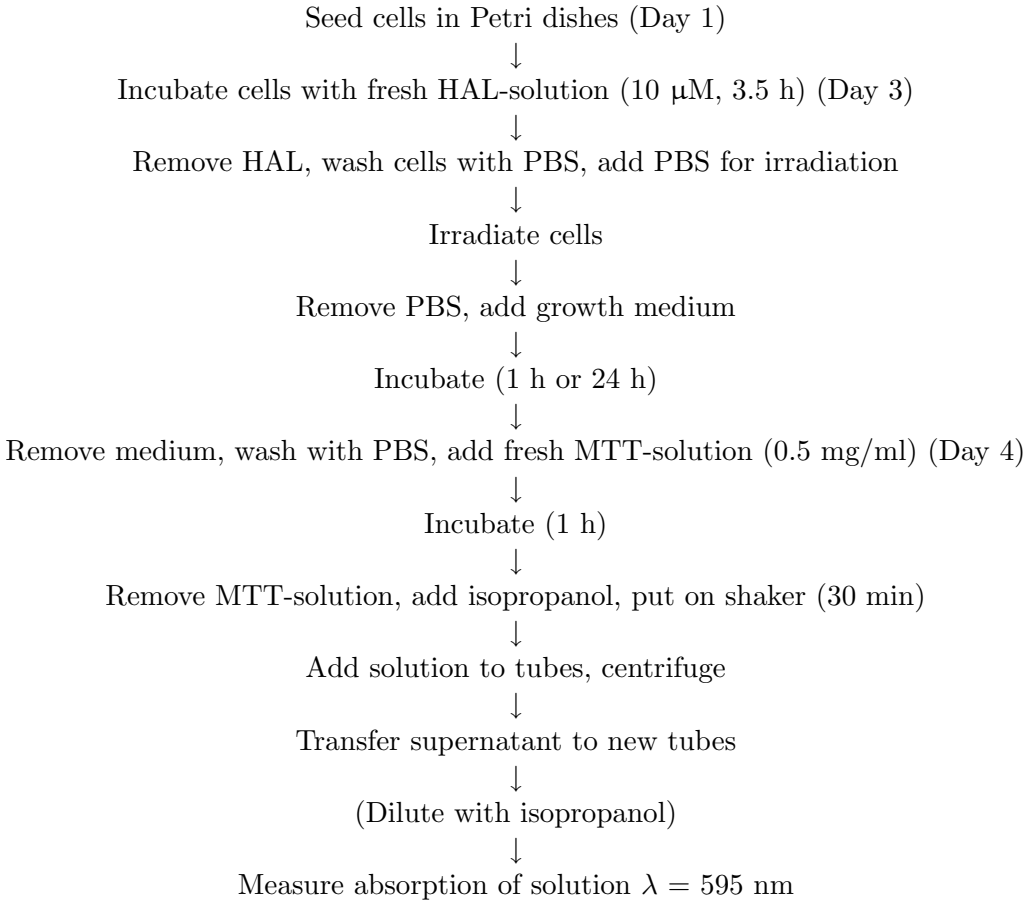

Figure 4.5: Protocol used for measuring survival of the AY-27 cells after HAL-PDT using the MTT assay.

4.5 Fractionated therapy

To study the effect of different forms of light delivery, it was decided to use the dose giving 50% cell death 1 h post PDT. This dose of 5.4 J/cm^2 corresponds to a light exposure time of 270 s. Inspired by Oberdanner *et al.* [46] we used (1) fractionated delivery with 45 s light and 60 s dark periods and (2) continuous light delivery. In addition we included a (3) split dose experiment with 135 s of light exposure, 300 s in the dark followed by another 135 s of light exposure.

Survival, apoptosis and necrosis was measured after 1 h and 24 h, both by the MTT assay and by flow cytometry using the Annexin V/PI method. The experiments are illustrated schematically in Figure 4.6.

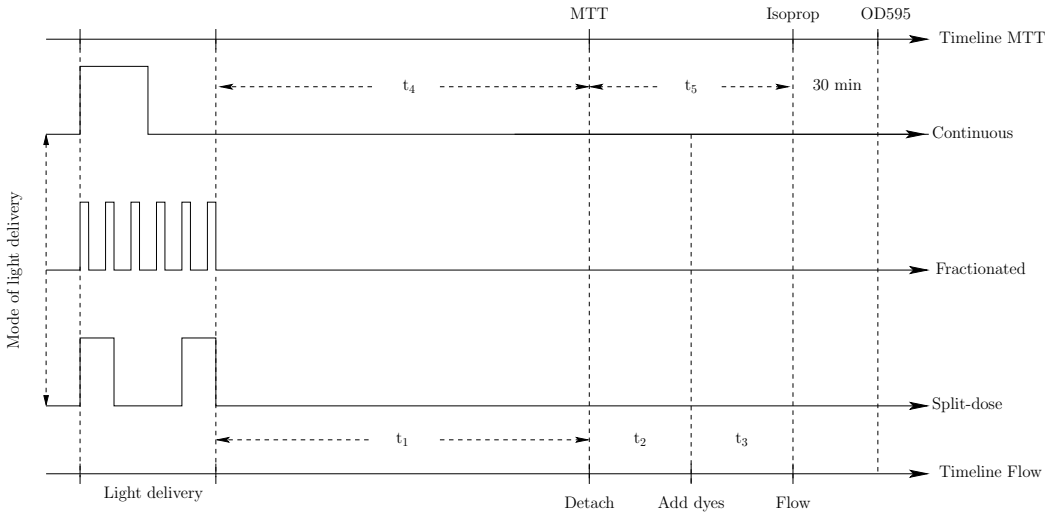

Figure 4.6: An overview of the experiments where fractionated and split light delivery is compared to continuous delivery. The timeline on top describes the experiment when survival is measured by the MTT assay, while the bottom line describes the experiment when survival is measured by flow cytometry. The three light delivery regimes shown are further described in this section. To get comparable results between the two methods, $t_1 + t_2 + t_3 = t_4 + t_5$.

Chapter 5

Results

5.1 A summary of the results from the pilot studies

There were many lessons to be learned from these early experiments, and with no previous experience in flow cytometry or confocal microscopy they provided the opportunity to learn the techniques. Experiences which influenced the treatment protocol and measurements of apoptosis and necrosis are briefly mentioned here:

Detachment of cells using Accutase: In earlier projects where AY-27 cells were treated with ALA and red light, cell aggregation after detachment with Trypsin/EDTA created problems for analysis through flow cytometry. As depicted in Figure 5.1, cell aggregation is not a problem when detachment is performed using Accutase. The detachment time for untreated cells at Day 3 was on average 12 minutes if seeded on Day 1 ($0.04 \cdot 10^6$/ cm^2) (data not included). Remarkably, the detachment time increased following HAL-PDT, and up to 20 minutes was needed to detach cells having recieved 5.4 J/cm^2.

Light dose: To discuss the type of cell death after treatment with any certainty, the treatment should give cell death ranging from zero to at least 90 percent. From Figure 5.2, we see that the cell survival is never under 75 percent, a level reached after a dose of 2.4 J/cm^2. We should therefore include higher doses to get more informative results. Also, as there were only small differences between the apoptotic levels one and four hours after HAL-PDT, 1 hour after treatment was chosen as the time to do measurements.

Detection of apoptosis: From the confocal microscopy images, such as shown in Figure 5.1, it seems that cells showing blebs characteristic for apoptosis, are frequently not tagged by the fluorochrome Annexin V Fluos, raising questions about the use of this method with the AY-27 cells. We decided to repeat the experiments using another assay for apoptosis to check for similar results.

Confocal microscopy studies: If the cells are not grown in wells suited for confocal microscopy, but need detachment before examination, it is only possible to focus on the cells that have sedimented to the bottom of the wells. We can not be sure

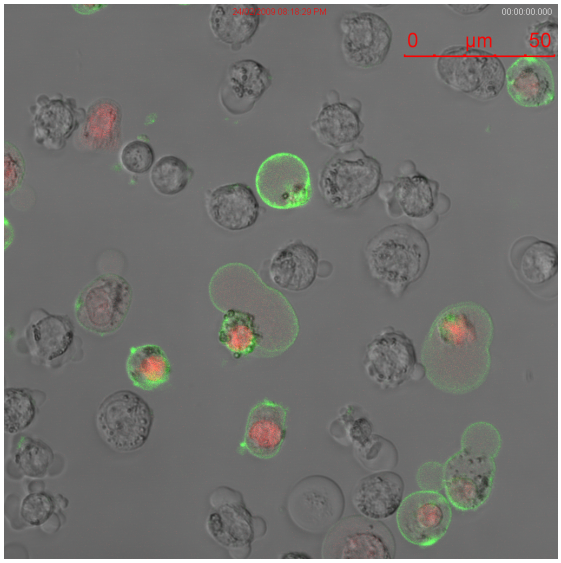

Figure 5.1: Confocal microscopy image of AY-27 cells 1 hour after red light HAL-PDT (3.5 h, 10 µM, 2.4 J/cm^2). The cells were handled as described in Figure 4.2, using Accutase to detach cells from the Petri-dishes before incubation with Ax/PI and loading in wells for confocal microscopy. The image clearly shows that PI (red fluorescence) is a nuclear dye, while Ax (green fluorescence) binds to phospholipides in the membrane. Still, cells having apoptotic morphology does not necessarily show any fluorescence. Cell aggregation, on the other hand, seems not to be a problem when accutase is used.

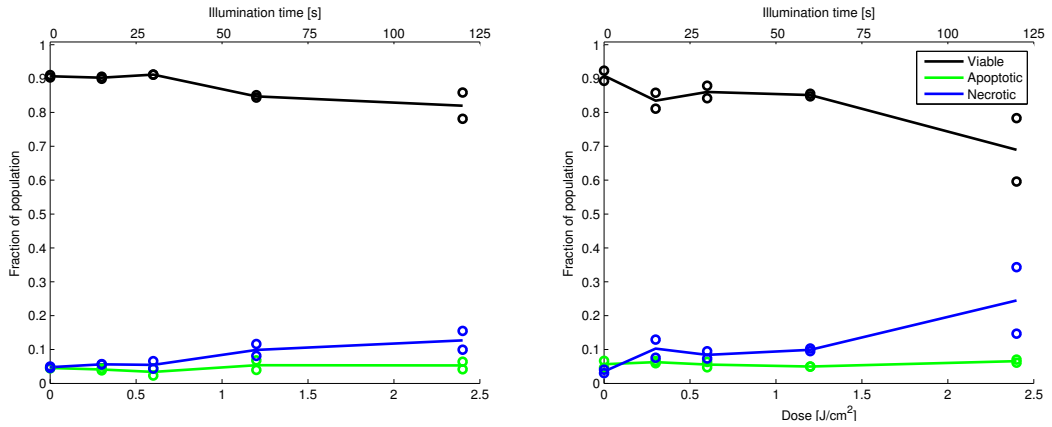

(a) 1 h post-PDT **(b)** 4 h post-PDT

Figure 5.2: (a): Viable, apoptotic and necrotic cells 1 h after HAL-PDT (10 µM, 3.5 h) as measured by flow cytometry with Ax/PI. (b): Viable, apoptotic and necrotic cells 4 h after HAL-PDT (10 µM, 3.5 h) as measured by flow cytometry with Ax/PI.

if the cells reaching the bottom is representative of the original population, as

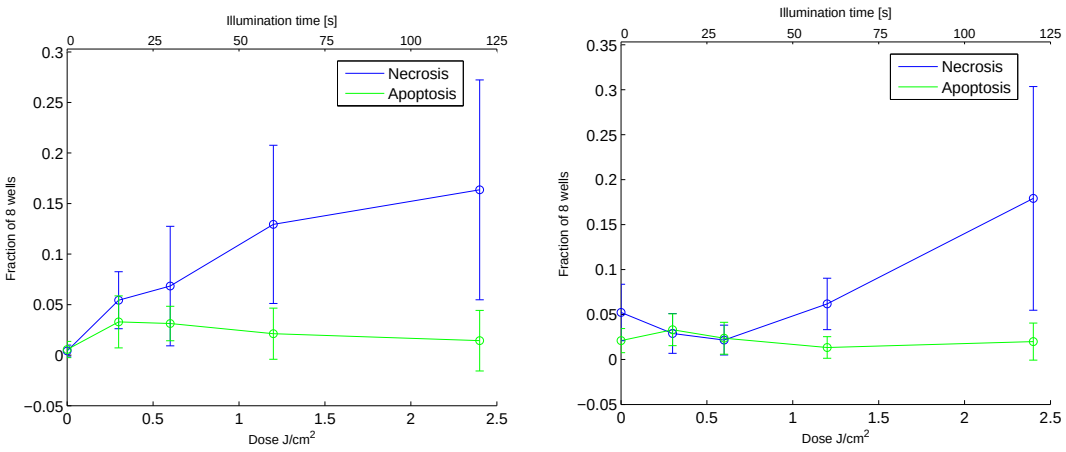

(a) 1 h post-PDT **(b)** 4 h post-PDT

Figure 5.3: (a): Apoptotic and necrotic cells 1 h after HAL-PDT (10 μM, 3.5 h), counted after confocal microscopy with Ax/PI. (b): Apoptotic and necrotic cells 4 h after HAL-PDT (10 μM, 3.5 h), counted after confocal microscopy with Ax/PI. Mean values and standard deviation is drawn at each point based on images from 2x4 wells.

there may be differences in the sedimentation properties of dead and viable cells. Secondly, cells which have been detached and handled much before inspection, will be structurally changed relative to cells treated and inspected when growing in their usual monolayer, which may influence the measurements. Figure 5.3 shows the measured apoptosis and necrosis after HAL-PDT on the AY-27 cells. The cells were detached with accutase after treatment and incubated with Ax/PI before inspection by confocal microscopy. The mean values both at one and four hours after treatment seem to correspond well with the flow cytometry results in Figure 5.2. However, the uncertainty in each point is large as the countings in each well never exceeded 100 cells, giving small variations a great influence on the result.

Several attempts were made using the protocol shown in Figure 4.3, where the cells are grown in wells two days before HAL-PDT and inspected by confocal microscopy. Unfortunately, we were not able to get any clear results with this method, as the cell death varied considerably between wells in the same well plate. The experiments were performed using several incubation times to avoid a queue of samples waiting to be analysed. This made the experiments extremely time consuming, and as the information obtained was of low quality, we did not continue using the confocal microscope for such quantitative studies. Examples of the images obtained can be found in Figure 5.4. Numerical data from these studies are not included, but the standard deviations are in the same range as shown in Figure 5.3.

Extracting information from the flow cytometer: The flow cytometer measures fluorescence from both fluorochromes in each passing cell, placing each cell in a 2D

plot based on the two parameters. This information provides a way to separate the population in viable, apoptotic and necrotic cells. The separation is done by the viewer of the data, and is therefore highly subjective. The following figures show how the populations are separated in this study using MATLAB, where all data from flow cytometry experiments were post-processed.

Instead of the 2D dotplots provided by the flow cytometer's software, density plots are shown. They give a better impression of the number of cells with the same fluorescent properties than dotplots, as the latter will have "blackouts" in areas containing many cells. Density plots were made by adding height information to the 2D (1024x1024) grid where each cell is placed during flow cytometry. Each grid point recieved counts from cells placed in that position, and the fluorescence from each cell also influenced the count in each of the eight neighbouring points, creating density information.

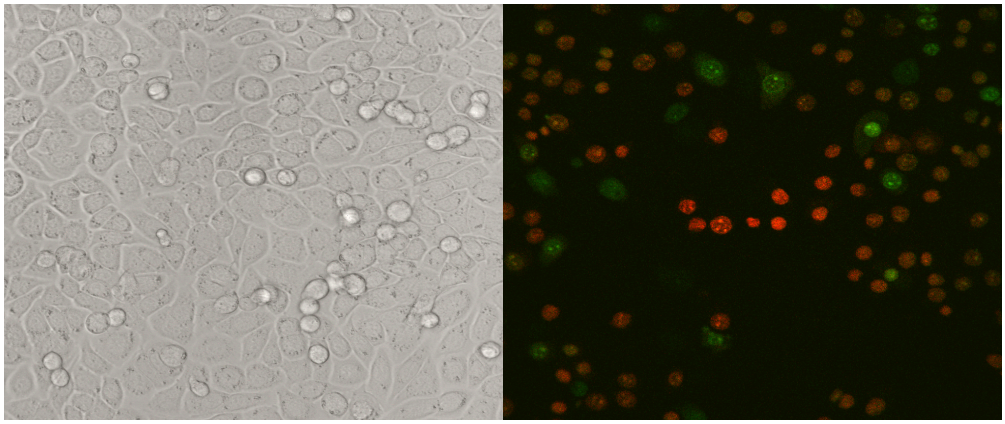

(a) Untreated cells **(b)** Only fluorescence (3.6 J/cm^2)

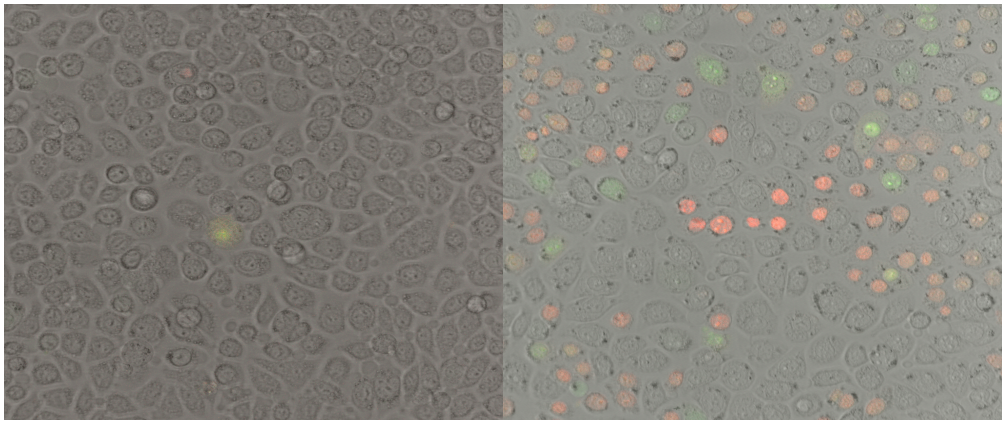

(c) Treated cells (1.8 J/cm^2) **(d)** Treated cells (3.6 J/cm^2)

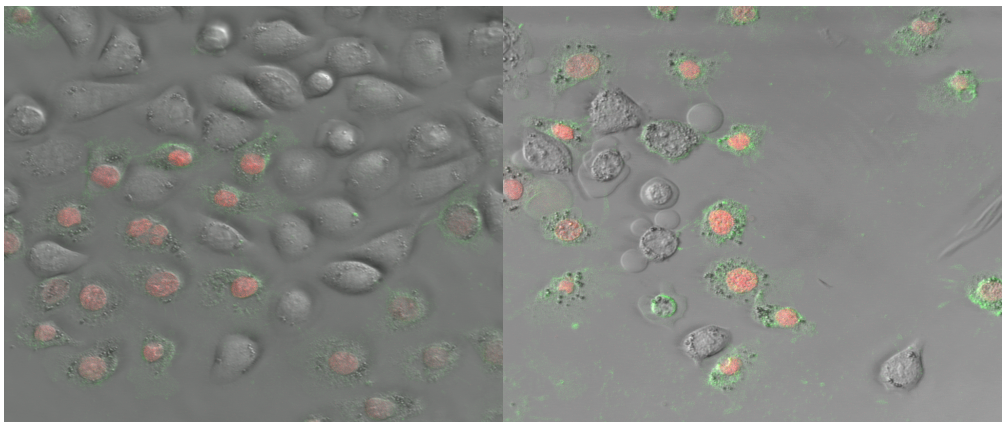

(e) Treated cells (1.8 J/cm^2) **(f)** Treated cells (3.6 J/cm^2)

Figure 5.4: (a): Shows healthy AY-27 cells, displaying their ability to adhere and use available space. (b): Fluorescence 1 hour after HAL-PDT using the fluorochromes YO-PRO-1 (green fluorescence) and PI (red fluorescence), illustrating that both are nuclear dyes. (c) and (d): Confocal microscopy images 1 hour after HAL-PDT using YO-PRO-1 and PI. (e) and (f): Confocal microscopy images 1 hour after HAL-PDT using Ax (green fluorescence) and PI.

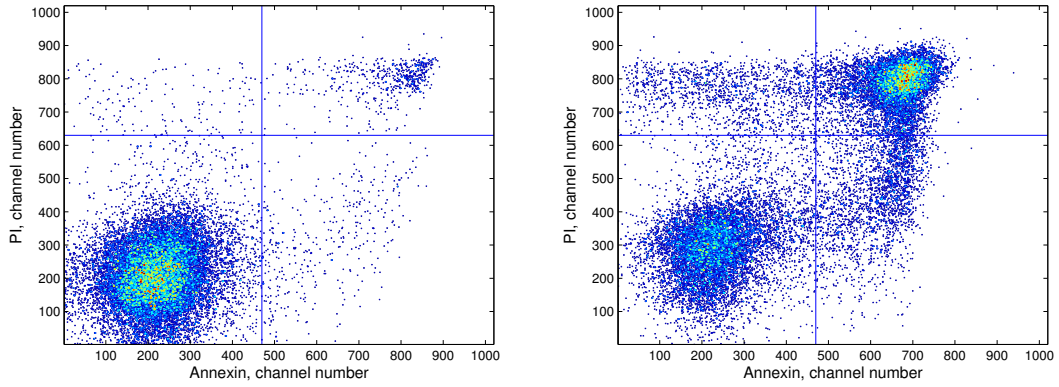

(a) Control **(b)** 6 J/cm^2

Figure 5.5: Results from flow cytometry displayed as density plots showing the results after 20000 counts for each sample. Fluorescence from Ax and PI are detected for each cell. Ranging from dark blue to red, density of cells range from lower to higher. The measurements are performed 1 h after HAL-PDT (10 µM, 3.5 h). Cells in the lower left quadrant are defined as viable, those in the lower right as apoptotic, while the two upper quadrants contain necrotic cells.

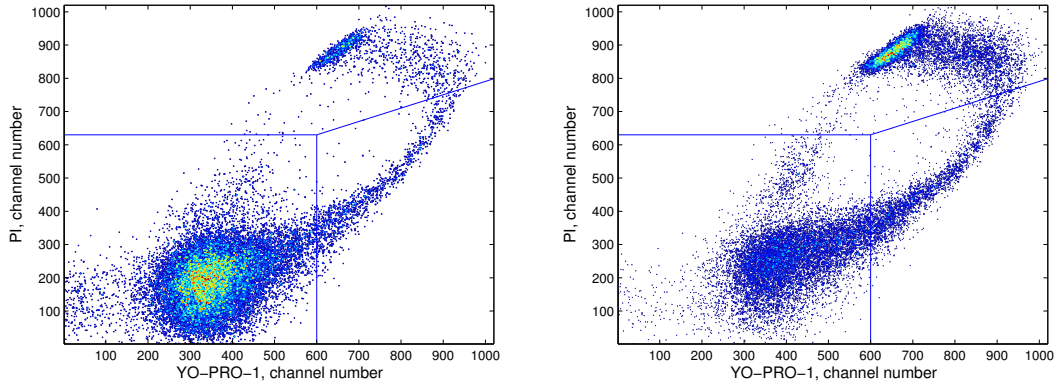

(a) Control **(b)** 6 J/cm^2

Figure 5.6: Results from flow cytometry displayed as density plots showing the results after 20000 counts for each sample. Fluorescence from YO-PRO-1 and PI are detected for each cell. Ranging from dark blue to red, density of cells range from lower to higher. The measurements are performed 1 h after HAL-PDT (10 µM, 3.5 h). As in Figure 5.5, the lower left region represents viable cells, the lower right region represents apoptotic cells and the upper region represents necrotic cells.

Alternative apoptotic marker:

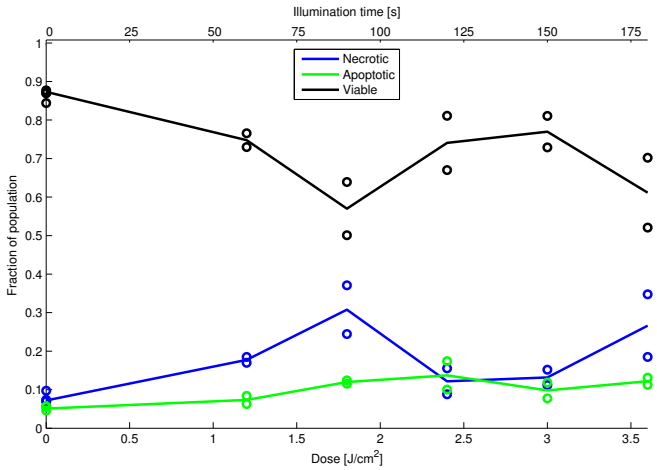

Figure 5.7: Viable, apoptotic and necrotic fraction of AY-27 cells 1 h after HAL-PDT (3.5 h, 10 μM) measured by flow cytometry using YO-PRO-1 and PI.

As Figure 5.7 shows, we did not detect any high apoptotic levels by using the the alternative fluorochrome either, though we did get a maximum value of 15% at 3.5 J/cm^2 which is larger than the values given by the Ax/PI method at any point (Figure 5.2a). Inspection of Figure 5.7 reveals a dip in survival at 1.8 J/cm^2, which is probably incorrect, as it is not likely that the survival curve has a local minima here. If these values are disregarded, the results using the two sets of fluorochromes are quite similar, though the apoptotic level seems slightly higher when using YO-PRO-1 and PI. Still, because it was even harder to separate the cells in viable, apoptotic and necrotic fractions (compare Figure 5.5 and Figure 5.6), and since the Ax/PI method is the most common of the two, it was decided to continue using the latter fluorochrome pair in the subsequent experiments.

5.2 Cell death following HAL-PDT with continuous light delivery

As Figure 5.8 and Figure 5.9 shows, cell death after HAL-PDT on AY-27 cells increases with increasing light dose. A shoulder region is observed in the survival curve 1 h post-PDT. The LD_{50} value 1 h after treatment was found to be 5.4 J/cm^2, corresponding to an irradiation of 4.5 minutes at 20 mW/cm^2.

As the dose increases the cells appear increasingly necrotic, while the apoptotic level is low and constant (about 4 percent) until a dose of 5 J/cm^2 is reached. Following a rapid change, it settles at a new constant level of 10 percent. The necrotic level rises earlier than the apoptotic level. From a background level of 4 percent in untreated samples, it reaches 10 percent already after 2 minutes of irradiation, and continues to rise until 90 percent necrosis is reached after 12 J/cm^2 (which equals 10 min of irradiation). Figure 5.9 gives the same information as Figure 5.8a, but with a linear axis and error bars. The measurement uncertainty is clearly largest at 6 J/cm^2. This is as could be expected, as the region between 5 and 10 J/cm^2 has the most rapid decrease in survival. Small changes in dose in this region will lead to large changes in survival.

Not only fluorescent light is collected by the flow cytometer. The laser beam used for excitation of the fluorochromes will be scattered by the passing cells, and this light is collected at small angles, forming the forward scattering signal often used to give an impression of cell size. In untreated cells, the size will have a simple gaussian distribution. In treated samples, the different populations present will give rise to a combined distribution as they swell or shrink. By averaging the forward scattered signal it is possible to get an impression of the dominant cell size in the sample. This is shown in Figure 5.8b. There seems to be an early increase in cell size for low doses, followed by a rapid decrease to a stable level reduced by a factor 2 compared to untreated samples.

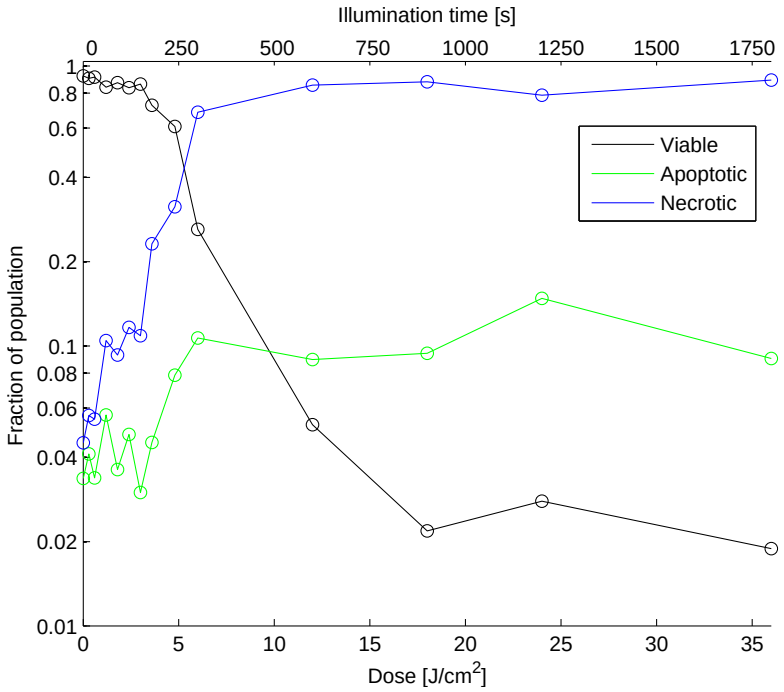

(a) Viable and dead cells

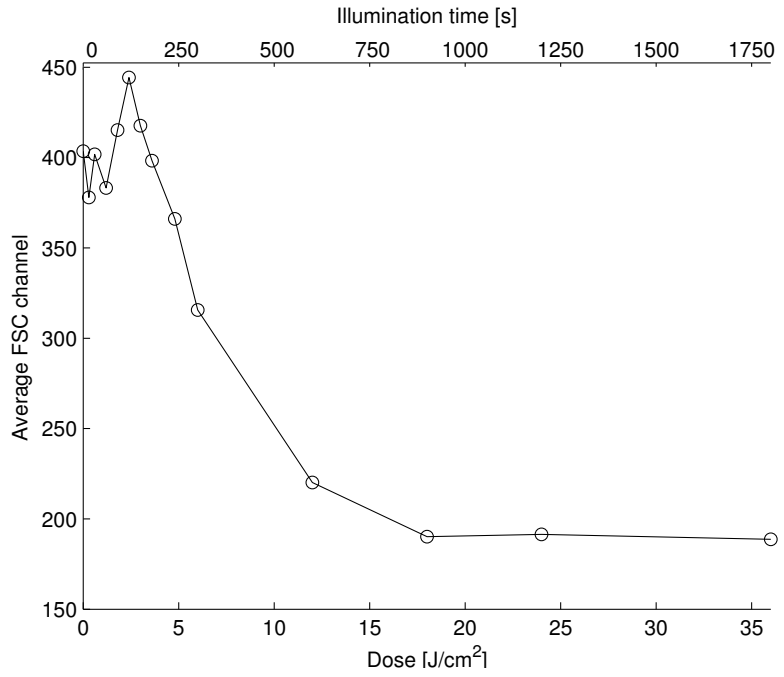

(b) A coarse measure of size

Figure 5.8: (a): Semilogarithmic plot showing dell death following HAL-PDT (10 µM, 3.5 h) on AY-27 cells measured by flow cytometry using Annexin V Fluos and Propidium Iodide to separate the population in three. Data points represent mean values from four separate experiments, each with two parallells. (b): The average forward scatter signal as a function of dose in the same experiment as (a).

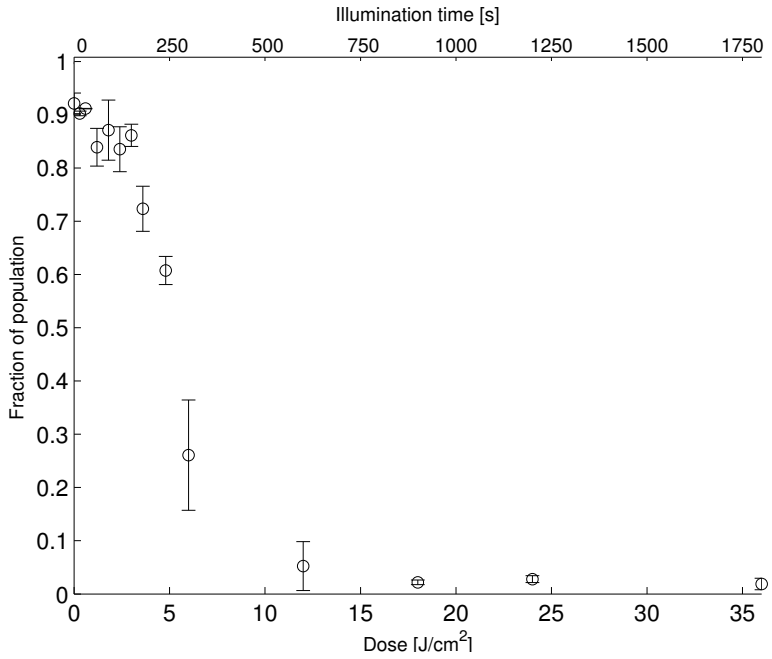

(a) Viable cells

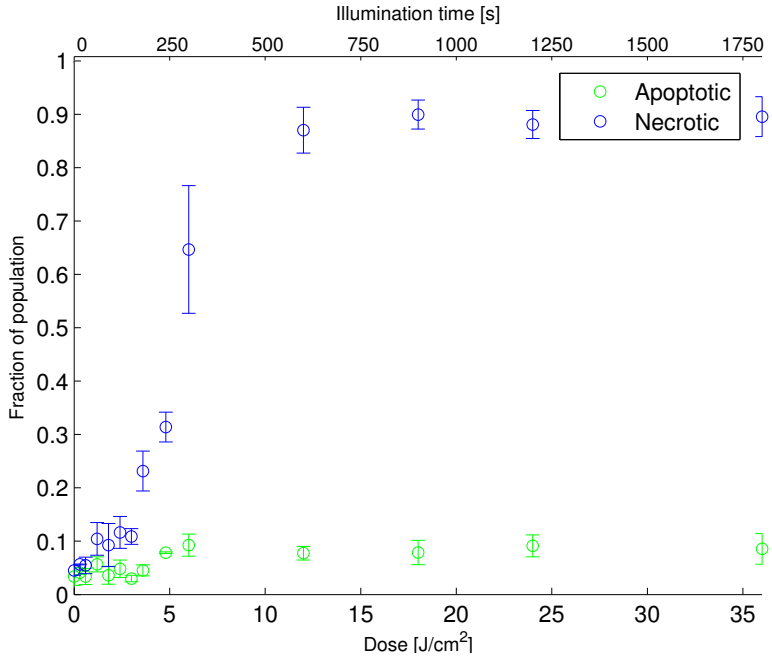

(b) Dead cells

Figure 5.9: Fractions of viable (a) and dead (b) AY-27 cells following HAL-PDT (10 μM, 3.5 h) measured by flow cytometry using Ax and PI to separate the population in three. Mean values ± standard deviation based on four separate experiments are given, each with two parallells.

By using the survival values measured by flow cytometry, originating from doses ranging from 0 to 12 J/cm^2, corrected to give 100 percent viability at $D = 0$, we can compare our results to theoretical survival curves derived from hit-theory as given in equation (2.2, page 17). These curves have two independent variables; the exponential slope of the survival curve, D_0, and the number of targets to be inactivated before a cell is killed, n. A third parameter, called the *quasithreshold value* ($D_p = D_0 \ln n$), is often used to describe the shoulder width. The parameter values which seemed to fit our data best is listed in Table 5.1. The resulting survival curves are plotted in Figure 5.10.

Table 5.1: Survival curve parameters

D_0 [J/cm^2]	n	D_p [J/cm^2]
2.5	4	3.5
2.5	5	4.0
2.5	6	4.5

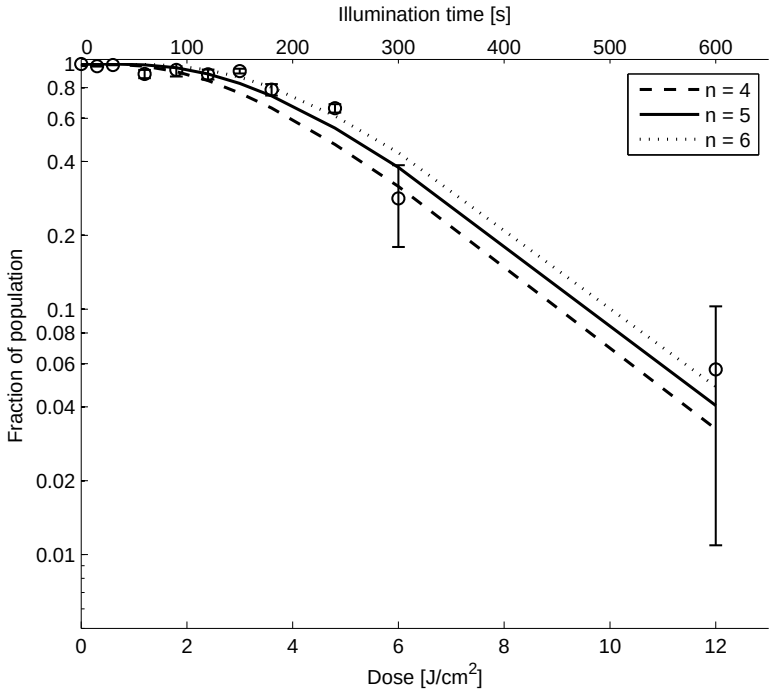

Figure 5.10: Theoretical survival curves from the single hit, multi target model is fitted to mean values with error bars from flow cytometry experiments as shown in Figure 5.8. The surviving fraction, $S = 1 - (1 - e^{-D/D_0})^n$ is plotted, where $D_0 = 2.5$ J/cm^2, and n is varied. Error bars seem large at higher doses, but this is just a result of the semilogarithmic axis.

5.3 Cell death following HAL-PDT with fractionated light delivery

As Figure 5.11 shows, fractionating the light delivery as defined on p. 33 did not affect the cells in the manner foreseen. Fractionating the dose giving 50 percent survival after 1 h gave no different results than continuous delivery. But splitting the dose in two, separated by a dark interval of 5 minutes, more than halved the surviving fraction. The trend is confirmed by both methods of detection — flow cytometry using Ax and PI, and the MTT assay, which measures mitochondrial activity. Intermediate results from absorption measurements are included in Appendix A.2, Figure A.2.

It also seems that the split dose method gives a higher level of apoptosis than the other means of light delivery (Figure 5.11b). The level is not high compared to the necrotic level, but it is the double of what is achieved by giving continuous or fractionated light delivery.

The viable fraction is measured relative to untreated control samples in the MTT assay while they are absolute values when measured by flow cytometry. The detection is also based on two very different mechanisms — mitochondrial activity in the MTT assay and *lack of* fluorescence in the flow cytometer. The measured values are therefore not expected to be identical. But when the trend is repeated in the two different types of experiments, it should give a good impression of the situation after HAL-PDT on the AY-27 cells both 1 hour and 24 hours after treatment.

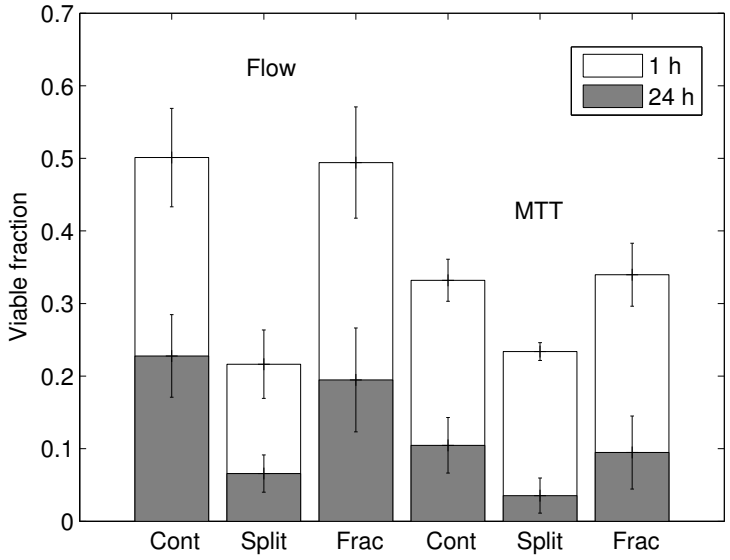

(a) Viable cells

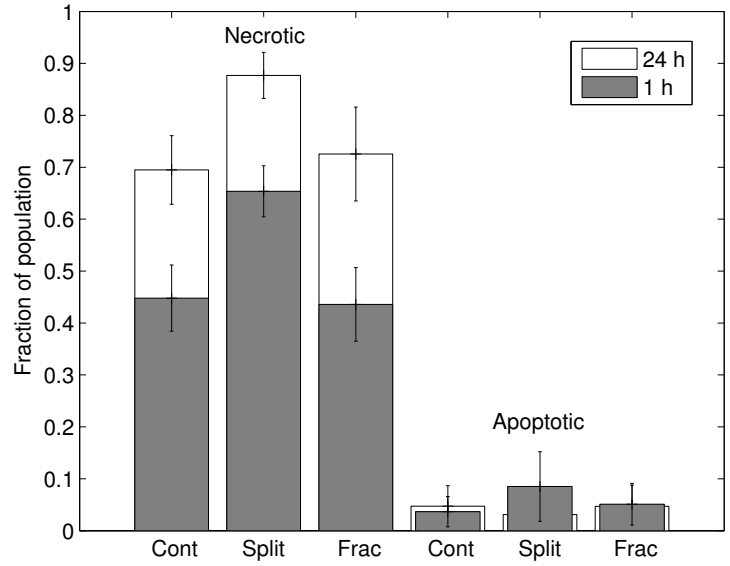

(b) Dead cells

Figure 5.11: (a): Viable fraction 1 h and 24 h after HAL-PDT (10 μM, 3.5 h, LD_{50}), measured by flow cytometry using Ax/PI. In addition, MTT viability results 1 h and 24 h after the same treatment are shown. (b): Apoptotic and necrotic fraction 1 h and 24 h after HAL-PDT (10 μM, 3.5 h, LD_{50}), measured by flow cytometry using Ax/PI. The bars represent mean values of 3 independent and identical experiments, each done in duplicates. Error bars give the mean value ± standard deviation. Notice that of esthetic reasons the post PDT times have been assigned different colors in the two figures.

Chapter 6

Discussion

6.1 Cell survival after red light HAL-PDT

In this study we were especially interested in the modes of cell death after HAL-PDT in AY-27 cells. As secondary apoptotic cells will be difficult to segregate from necrotic cells, we based the dose-response curves on measurements done approximately 1 h after treatment. Because the flipping of phosphatidylserine from the inner to the outer lipid layer occurs early in apoptosis [43], we should be able to detect apoptotic cells with the Ax/PI method.

As will be discussed later, there may be some problems with the specificity of the Ax/PI method for detection of apoptosis. Still, the surviving cells, excluding both dyes, should be adequately represented also by this method. This can be seen in the untreated samples where the measured fraction of viable cells is larger than 90 percent, which is a reasonable estimate of the amount of viable cells in a population. The survival curve obtained in this study can thus be compared to survival curves obtained also by other methods, such as the MTT assay.

6.1.1 Comparing experimental survival curves

When comparing survival curves, it is important to remember that wavelength and irradiance influence the survival of the cells. As the absorption spectrum of PpIX in Figure 2.4 shows, the absorption is three times as efficient at 435 nm (blue light) compared to 630 nm (red light), increasing the probability per second for exciting a PpIX molecule into a triplet state which can react with oxygen. This probability per second will also increase by increasing the light irradiance.

In the project work performed last semester [47], a survival curve for the AY-27 cells 24 h post HAL-PDT was established using the MTT assay. The experiments were performed using the same light source and the same photosensitizer concentration, but with different irradiances. The survival curve from the former experiments, using an irradiance of 36 mW/cm^2, was comparable to HAL-PDT (10 μM, 3.5 h) on AY-27 cells using blue light (435 nm, 12.9 mW/cm^2) [48]. These survival curves decrease rapidly, without an initial shoulder region (or a much smaller shoulder), giving an appearance of a single hit, single target system. If the survival curve shown in Figure A.1, Appendix

A.1, is compared to results from blue light experiments performed by Linda Helander [48], it is evident that equal dose using red or blue light gives equal treatment outcome *in vitro*, if a correction for absorption is included in the results. The LD_{50} dose was 1.15 J/cm^2 after 24 hours for red light, three times the value for blue light experiments: 0.38 J/cm^2. This corresponds to the absorption of light being three times as efficiant at 435 nm than at 630 nm.

Figure 5.8a illustrates that decreasing the red light irradiance from 36 mW/cm^2 to 20 mW/cm^2 produces survival curves which tell another story — not simply a single hit, single target situation. Ionizing radiation used *in vitro* can produce similarily shaped survival curves, and the shoulder region is explained both by sublethal damage repair and the need for several "hits" to produce lethal damage [38]. Enzymatic repair of single or double stranded DNA breaks is established as able to produce an initial shoulder, and fractionating or splitting the radiation dose will cause the shoulder region to repeat, thus causing the overall survival to increase.

Figure 5.11a shows a *decrease* in cell survival when the LD_{50} (1h post PDT) is split in two separate fractions — the opposite of what would be expected if sublethal damage repair was active in the dark period. The initial shoulder of the survival curve combined with the decrease in survival in split-dose experiments give indications that sublethal damage repair is not an important mechanism in photodynamic treatment as performed in this study. The shoulder would then be a result of the fact that several targets in a cell need to be hit to produce sufficient damage for cell death.

6.1.2 Comparison to theoretical survival curves

As the dose increases, the survival curve from the single hit, multi target model (Eq 2.2) approaches a single exponential. This exponential will of course decrease towards zero at high doses. The number of targets that need inactivation, denoted n, can be estimated in a semilogarithmic plot by extending the linear part of the survival curve to find the intersection with the y-axis, after fitting the single hit, multi target survival curve to the experimental data.

$$\begin{aligned} S &= 1 - (1 - e^{-D/D_0})^n \\ &= 1 - (1 - ne^{-D/D_0} + \frac{n}{2}e^{-2D/D_0} + ...) \xrightarrow{\text{Large } D} ne^{-D/D_0} \end{aligned} \tag{6.1}$$

As seen in Figure 5.10, the survival curve obtained in this study resembles single hit, multi target survival curves up to a dose of 18 J/cm^2, where the measured survival, as shown in Figure 5.8a, reaches a constant level of 2-3 percent. This level does probably not represent a true fraction of the population, which would mean that 3 percent of the cells are resistant to photodynamic therapy. More specifically, they are able to survive doses up to 36 J/cm^2. Although some cells may be more resistant, a survival of 3 percent at 36 J/cm^2 is much larger than the 0.8 percent value at 36 J/cm^2 found by the MTT assay last semester, Appendix A.1, Figure A.1b.

One explanation of the difference in survival between the two methods, could be the combination of samples consisting mostly of cell fragments and the threshold of detection in the flow cytometer. Fragments giving an FSC signal under a certain value will not

be regarded as cells, and are not counted. This will lead to an overrepresentation of viable cells in the measurement, as the very few living cells are always counted, while the vast majority of the necrotic cells will go unnoticed. Based on the assumption that the survival curve should approach zero at high doses, the fitted curve in Figure 5.10 did not use data corresponding to doses over 12 J/cm^2.

It is important to remember that the results from curve fitting only present one small version of the truth. The single hit, multi target model does not differentiate between apoptotic and necrotic cell death, or between apoptotic and necrotic targets. It estimates the number of targets of any kind that need inactivation before the cell dies. How the curve is fitted to the experimental data is also important. Is the shoulder or the slope more important?

In Figure 5.10, a good fit to the slope was stressed. If all points are considered equally and a nonlinear least squares fit is performed, the estimate of the number of targets and the shoulder width is changed to approximately $n = 10$ and $D_0 = 2$ J/cm^2. The curve and experimental data points are shown in Figure 6.1.

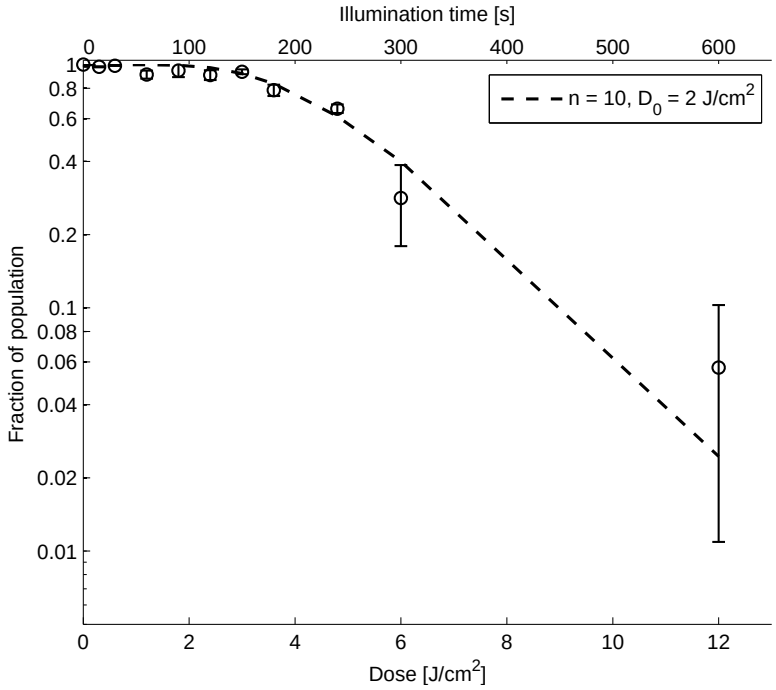

Figure 6.1: Alternative surivival curve parameters used to fit a single hit, multi target curve to survival data from flow cytometry 1 hour after red light HAL-PDT. Mean values are given ± standard deviation. Error bars seem large at higher doses, but this is just a result of the semilogarithmic axis.

This may look like a good fit, but if the parameter values are given with 95% confidence intervals as in Table 6.1, the impression may change. Still, the quasithreshold value is similar to what we obtained with n = 6 and D_0 = 2.5 J/cm^2, demonstrating that one shoulder width can be obtained by different combination of survival curve

parameters.

The single hit, multi target equation has been used with experimental data from ALA-PDT on WiDr cells [41]. Their estimate of the number of targets to be inactivated before a cell is killed at 37 °C was $n = 11 \pm 2$. Although this value is similar to the value in Table 6.1, the cell lines are different, and one cannot simply assume that the same number of lipid or protein inactivations will lead to cell death in both of them.

Table 6.1: Alternative survival curve parameters

Parameters:	D_0 [J/cm^2]	n	D_p [J/cm^2]
Estimated values:	1.89 (1.14, 2.64)	10.41 (0, 21)	4.43
Used in Figure 6.1:	2	10	4.6

We can conclude that the single hit, multi target model is not a perfect match for our data. But if we were to test different treatment conditions (such as irradiance, temperature or others) over a range of doses it would be convenient to use the model for calculating parameters which again could be used in comparing different outcomes. An example could be different shoulder widths, which could indicate different ability to accumulate sublethal damage under the different conditions.

6.2 The modes of cell death after HAL-PDT

As PpIX is formed in the mitochondria of eukaryotic cells, it seems reasonable that HAL-PDT should lead to apoptosis through the activation of the mitochondria mediated pathway, discussed on p. 10. Our results from flow cytometry using Annexin V Fluos and propidium iodide does not support this theory, but indicate that necrosis is the most important way of cell death following HAL-PDT. This could mean that mitochondria is not the primary targets in our experiments, which leaves the plasma membrane as a possible replacement. If the oxidative damages to lipids and proteins in the plasma membrane dominates the lethal damages in a cell, necrosis will follow. Support can be found at several levels:

6.2.1 Indications of necrosis as dominant mode of cell death

PpIX localization:

Even though PpIX is formed in mitochondria, it rapidly diffuses to other intracellular membrane sites such as lysosomes and the plasma membrane [49]. Fluorescence microscopy studies of AY-27 cells 3 h and 4 h after incubation with HAL (1 μM) clearly shows accumulation of the lipophilic sensitizer in the plasma membrane [35]. In this study an incubation time of 3.5 h is used, which based on these former results should lead to a highly sensitised plasma membrane. Sufficient oxidative damages to molecules in the plasma membrane (e.g. lipid peroxidation) will induce necrosis by loss of plasma membrane integrity [18].

Altered adhesive properties:

Cell adhesion proteins, such as integrins and cadherins are integrated in the plasma membrane. Since singlet oxygen acts in the immediate vicinity of its formation, these proteins may be damaged if the photosensitizer is present in the lipid bilayer. The adhesive properties of WiDr and D54Mg cells after ALA-PDT have been studied [50], and it was found that direct effect on the plasma membrane influenced the adhesive properties of these cell lines. Even sublethal damages influenced their adhesive properties, making them more resistant to trypsination.

Although we have not studied the adhesive properties of the AY-27 cells by any sophisticated method here, we have experienced that there is a large difference in their resistance to detachment by Accutase before and after HAL-PDT. This suggests that oxidative damages to proteins in the cell membrane may be an important effect in the AY-27 cells after HAL-PDT (3.5 h, 10 μM, 630 nm).

Indications of an early increase in cell size:

Although one should be careful in interpreting the forward scattered (FSC) light detected in flow cytometry as a clear measure of cell size, the average FSC signal as a function of PDT dose, shown in Figure 5.8b, seem to support that necrosis is the dominant way of cell death following HAL-PDT with our conditions.

Untreated samples show a simple gaussian distribution, averaging at a lower value than samples which are given low PDT doses. At these low doses, Figure 5.8a shows little cell death, which means that PI has not yet penetrated the cell membrane to a large extent. Increase in cell size and an intact cell membrane are features characteristic of early necrosis or oncosis, where the cell swells — the opposite of apoptotic cells which will shrink. The increase in FSC signal could then reflect a dominant early necrotic population. As the dose passes 15 J/cm^2, the average FSC signal ceases to decrease, having reached a level corresponding to near total extinction of the cell population. Observations in the confocal microscope confirmes that such high doses will lead to "pulverization" of the cells, already 1 h after treatment.

The influence of an apoptotic window:

The dose range where the damage is too serious to allow repair of the cell, but not severe enough to endanger the cellular ion homeostasis, can be referred to as the *apoptotic window*. This window is influenced by the treatment protocol through parameters such as incubation time, concentration of photosensitizer and the irradiation regime [23]. In this study we have used the precursor concentration shown to give maximal PpIX concentration in the cells after 3.5 h incubation, as found by Odrun Arna Gederaas and Linda Helander at the Department of Cancer Research and Molecular Medicine at NTNU, which simplifies comparison of the results.

If we had used another treatment protocol, giving a lower concentration of photosensitizer or an even lower light irradiance, the level of treatment induced apoptosis could increase, as we then might enter into the range of the apoptotic window. Others have demonstrated that it is possible to induce apoptosis in the AY-27 cell line with *hypericin-PDT*, but it is highly dependent on the concentration of the photosensitizer

and the time of observation. At low concentrations of the photosensitizer, a dose of 1.8 J/cm^2 (2 mW/cm^2, 595 nm) prevalently induced apoptosis, while the same dose given after incubation of slightly higher concentrations of hypericin prevalently induced necrosis [51]. From our studies, it seems that giving 10 μM of HAL 3.5 h before irradiation with red light of 20 mW/cm^2 is not the best way of inducing apoptosis in the AY-27 cell line.

6.3 A discussion of the methods and possible impacts on the results

6.3.1 Are we missing the apoptotic cells?

The indications of necrosis as the dominant mode of cell death after red light HAL-PDT are many, as our experiments fail to give us the evidence of an apoptotic level higher than 10 percent after treatment. Still, if Figure 5.11 is studied, some questions about the Ax/PI method arise. Among others, the discrepancy between the measured apoptotic level and the mitochondrial activity 1 h and 24 h after treatment should be discussed.

First, take a look at Figure 5.11b. There is approximately a 25 percent difference between the necrotic level 1 hour and 24 hours after treatment. As necrosis arises shortly after treatment, one would not expect such a large difference. The increase could be explained if the level of apoptotis had decreased correspondingly, because cells which are apoptotic after 1 hour are expected to reach a necrotic stage after 24 h. But this is not seen here, as the apoptotic level is nearly unchanged. This may indicate that the level of apoptosis measured 1 h after treatment is too low.

Secondly, look at Figure 5.11a. The MTT assay measures mitochondrial (metabolic) activity, and according to Plaetzer *et al.* [23], the temporal dynamics of the mitochondrial activity will reflect the apoptotic fraction of cells after $AlPcS_4$-PDT when measured 3 and 24 hours after treatment. Our MTT results show a dramatic change in metabolic activity in the cell population 1 hour and 24 hours after treatment. 1 hour after treatment, about 35 percent of the cell population show the ability to convert MTT to formazan after continuous delivery of the LD_{50}[1] dose. 24 hours after treatment, only 10 percent are able to do the same. According to Plaetzer *et.al*, the difference between the two measurements represents the apoptotic fraction of the population. If this is true in our system also, we may have greatly underestimated the apoptotic fraction by using the Ax/PI method.

6.3.2 Timing

In our experiments, measurements are done by definition 1 hour and 24 hours after treatment. These post-PDT times were chosen as the most important, as it is impossible to investigate all points in time after treatment. The true time of measurement is not exactly as defined though, because the measurements are not done instantaneously. This is illustrated in Figure 4.6. After treatment, the samples are left undisturbed for one hour (or 24 h) in normal cultivation medium. If they are to be studied in the flow cytometer, they need detachment (20 min), centrifugation (3 min) and incubation with

[1] Defined 1 hour after treatment

Ax/PI (15 min). Including working time, the time from treatment to measurement approaches 2 h.

If the cells are to be studied by the MTT assay, they are also left undisturbed for one hour (or 24 h) and incubated with the MTT solution (1 h) before the formazan is solved in isopropanol. At that stage though, the cells will die, and the time spent after addition of isopropanol is not as important. It is the amount of formazan produced before the addition of isopropanol that gives information of how and when the cells die. Both methods then lead to a time of measurement of *2 hours* after treatment, where 1 hour is spent undisturbed. It is unclear exactly how treatment post-PDT, such as detachment or incubation with the MTT solution, influences the normal post-PDT processes in the cell. But if processes such as cell repair continue during this treatment, the true time of measurement is not 1 h post-PDT, but 1.5 - 2 h (and $\approx$ 25 h) post-PDT .

The execution of apoptosis may take several hours [52], and although PS exposure happens at an early stage [43], we may have missed the event by measuring earlier than 2 h after treatment. However, this reasoning is contradicted by the results from the pilot studies with Annexin V Fluos and propidium iodide shown in Figure 5.2, which *did not* reveal any large differences in the apoptotic level 1 h and 4 h after PDT. Still, these doses were small, ranging only from 0 to 2.4 J/cm^2. Also, at the largest dose, the fraction of viable cells was as high as 75 percent 4 h after treatment.

HAL-PDT has been found to effectively induce apoptosis in human leukemia cells (5 µM, 4 h, 8 mW/cm^2, 450 nm, Furre *et al.*) [53], where cellular shrinkage and peripheral chromatin condensation were displayed from 4 h after treatment. 20 h after a dose of 160 mJ/cm^2, more than 80 percent of the population was characterized as apoptotic, as found from fluorescence microscopy images. Furre *et al.* suggest that mitochondria initiated — and perhaps also cell surface death receptor induced, pathways of caspase activating cascades *are not* involved in the induction of apoptosis by HAL-PDT. *The apoptosis inducing factor* (AIF) which is released from mitochondria and translocated to the nucleus was investigated in their study and was suggested to play a central role in a caspase (and cytochrome C) independent induction of apoptosis. As the translocation from the mitochondria to the nucleus via the cytosol takes time, the highest apoptotic level was found 20 hours after treatment, with approximately 55 percent reached after 6 hours. This slow progression is consistent with the results of another study by Wyld *et al.* [54], where the apoptotic level after ALA-PDT (1 mM, 4 h, 350-450 nm, 86.5 mW/cm^2, LD_{50}) on human bladder carcinoma cells was largest after 8 hours, reaching a level of 55 percent.

6.3.3 A reconsideration of the Ax/PI assay

There are some problems regarding the use of the Ax/PI assay to detect apoptosis, especially when used with adherent cells. According to Lecoeur *et al.* [21], the Ax/PI assay does not discriminate between apoptosis and oncosis. In addition, the detachment process can cause mechanical damages to cells which can lead to false positives.

The first problem should cause an overestimation of the apoptotic population, but that does not seem to be a problem here, as our measurements of the apoptotic fraction is rather low. The second problem should lead to an overestimation of the necrotic population. This could be a problem, if we by detaching the cells make them permeable

to the fluorochromes. Still, this should be evident also in control samples, and the results from flow cytometry does not show a high necrotic or apoptotic level in the untreated samples. In fact, the control samples come out as 95% viable, indicating that most of the cells remain viable also after the detachment process. If this is not the case, the fluorochromes are extremely inefficient in binding to their substrates.

It is difficult to conclude whether or not the lack of apoptosis measured by the Ax/PI assay reflects lack of apoptosis in the cell population after red light HAL-PDT. The measurement technique is never perfect, and there is no general kinetic model of how cells react to photodynamic therapy. As much is unknown about the response of the AY-27 cells to PDT, and as the time of measurement post PDT seems to be important (discussed on p. 54), the cell population should be followed over time, instead of just the two time points we were able to study here.

Including other markers of apoptosis in future experiments, such as disruption of the mitochondrial transmembrane potential ($\Delta\Psi_m$), would be useful. The collapse of the transmembrane potential during apoptosis can be studied by flow cytometry or confocal microscopy by using the $\Delta\Psi_m$ sensitive dye JC-1[2] [53]. Reliable conclusions about the amount and kinetics of induction of apoptosis in the AY-27 cell line after HAL-PDT should be supported by several methods, not only results from one apoptotic marker, such as the display of phosphatidylserine.

6.3.4 Conditions before and during treatment influence the outcome of PDT

After incubation with HAL, the cells are washed in PBS. They stay in PBS before and during light delivery, but because of the experimental protocol in the fractionation and split-dose experiments, the time spent in the incubator with a 5% CO_2 content varies between 5 and 30 minutes before irradiation. As Figure 6.2 shows, this may influence the outcome of treatment at long irradiation times, such as those used to obtain a dose of 5.4 J/cm^2 in a split-dose experiment. Results from earlier experiments show that the incubator time is not as important at lower doses.

Results from the fractionation and split-dose experiments are found in Figure 5.11. One hour after treatment the survival is *lower with a factor of two* in the split-dose samples compared to those where continuous or fractionated irradiation is given. As this result was unexpected, it was decided to test a hypothesis that the time in the incubator before treatment could influence the treatment outcome. Figure 6.2 shows the results of a split dose experiment where 5.4 J/cm^2 has been delivered in two equal fractions to all samples, but the time spent in the incubator before treatment is different. One hour after treatment, 50 percent of the cells which were incubated 15 or 30 minutes before treatment were viable compared to only 25 percent of the cells with the shortest incubation time.

In the fractionation experiments, the split-dose samples were treated first, after 5 minutes in the incubator. If the effect seen in Figure 6.2 is included, it leads to the conclusion that the treatment outcome is not changed between the three modes of light delivery tested in this study. The difference in survival must have its origin somewhere else.

[2] A J-aggregate forming lipophilic cation [55]

After the cells have been washed and left in PBS, they will experience the pH and gas concentrations as given by the buffer solution. PBS, *phosphate buffered saline*, contains phosphate compounds instead of carbonate compounds to avoid pH changes when working in atmospheric conditions, and pH changes should thus not be a problem. Because the concentration of CO_2 in the incubator and the atmosphere (air) is respectively 5% and 0.03% [56], disturbances in the amount of oxygen and carbon dioxide present in the PBS could influence the treatment outcome, as oxygen is a limiting factor in the PDT treatment and CO_2 is a singlet oxygen quencher [57]. In addition, the cells with the shortest stay in the incubator may still be recovering from mechanical stress following the washing procedure, and could be more sensitive to oxidative damages than normal.

Although these are only speculations, the fact remains that there is a difference in the outcome of PDT between samples incubated for different times before treatment, where a stay of only 5 minutes in the incubator seem to reduce the cells ability to survive compared to incubation times of 15 or 30 minutes.

6.4 The effects of fractionated irradiation

Contrary to what we expected, we found no difference in PDT efficacy between fractionated and continuous light delivery. The treatment regime consisting of light/dark/light intervals of 45 s/60 s/45 s until the LD_{50} dose was reached, was inspired by a study performed by Oberdanner *et al.* [46], where a *decrease* in PDT efficacy was found when the light delivery was fractionated in this manner. They found that PDT doses leading to 10 percent mitochondrial activity (measured by the MTT assay) 24 h after treatment with continuous light delivery, lead to 20 percent survival when fractionated irradiation was used. The study was perfomed using the lipophilic, singlet oxygen generating photosensitizer *hypericin* on the adherent cell line A431, which resembles the situation in our system. It was suggested that fractionated therapy *in vitro* is influenced by the recycling of GSH by glutathione reductase during the dark intervals. GSH is a ROS quencher and if recycled it could explain the increase in survival levels when fractionated irradiation was used compared to survival after treatment with continuous irradiation.

The increase in survival was not seen in our study, indicating that the recycling of GSH is not as efficient in our system. Maybe the glutathione reductase is itself damaged by ROS? Still, there may be an underlying effect of GSH, which could be determined by adding BCNU, an inhibitor of glutathione reductase, to the cultivation medium before irradiation. If the survival then decreases compared to samples without BCNU, the effect of GSH recycling is demonstrated. Without having performed such an experiment, one could still suggest that factors that should increase PDT efficacy, such as regeneration of PpIX and reoxygenation in the dark intervals, were counteracted by a mechanism such as GSH recycling — leading to equal survival with continuous and fractionated light delivery in our experiments. On the other hand, depletion of oxygen is not likely to be a problem *in vitro*, as there is continuous gas exchange between the supernatant and the outside air.

Sublethal damage repair could also influence the outcome of fractionated therapy, as repair mechanisms could be active in the dark intervals. Still, repair is not assumed to happen in dark intervals of only 60 s, and should not be influencing the results of the fractionated regime to a large extent.

It seems from our results that a dark period of 5 minutes does not have any significant influence of repair processes either, as the survival was equal between samples recieving fractionated and split-dose PDT.

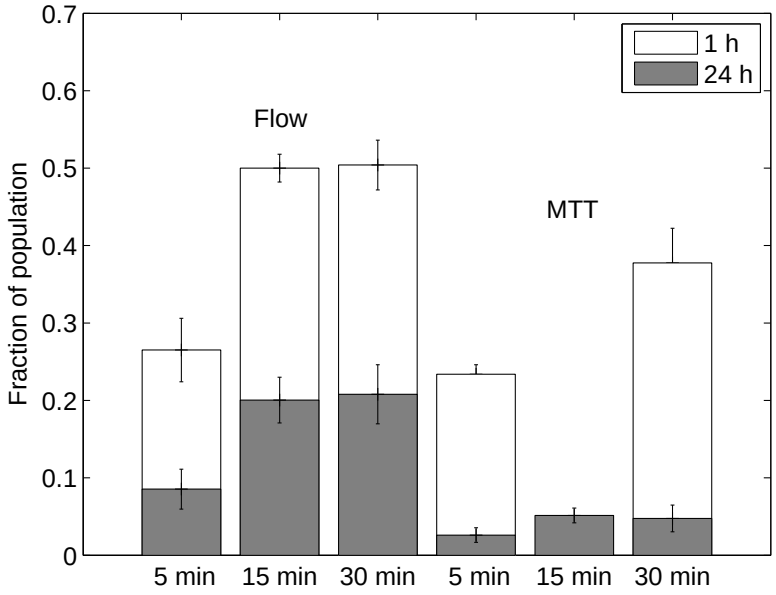

(a) Viable cells

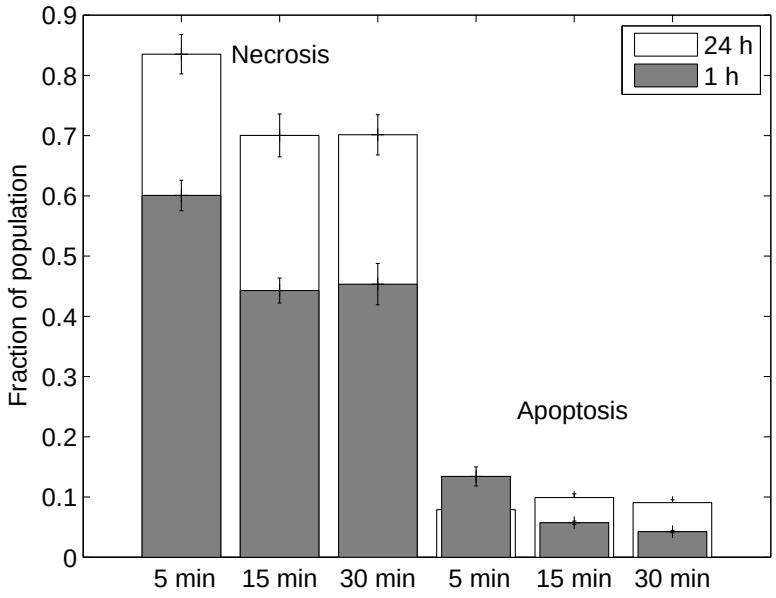

(b) Dead cells

Figure 6.2: Results of a red light HAL-PDT (10 μM, 3.5 h) split-dose experiment (135 s light, 300 s dark, 135 s light). The samples were kept in their regular incubator with 5% CO_2 5, 15 or 30 minutes before treatment, and the viability measured 1 hour and 24 hours after treatment. MTT results for (1h, 15 min) is missing due to lack of data at this point. Notice that of esthetic reasons the post PDT times have been assigned different colors in the two figures.

Fractionated therapy *in vivo*

In vivo, fractionation has been found to both increase [58] and decrease PDT efficacy [59]. By measuring the partial oxygen pressure, pO_2, effective reoxygenation schemes using ALA-PDT has been shown to require dark intervals of 150 s [60], while others again report that several hours is needed [61]. As the results differ to a large extent between the investigators, timing of the dark interval(s) is probably influential for the outcome and further optimization is needed. By studying the effects of fractionation *in vitro*, the direct *cellular* mechanisms determining the treatment outcome can be revealed. These results cannot be translated directly all *in vivo* situations, as the effect of tissue oxygenation may be more influential for the PDT efficacy. But for well oxygenated tumors, *in vitro* results may give important information about response to PDT.

6.5 Future work

If someone is to continue the red light PDT studies on the AY-27 cell line, some changes in the protocols could be recommended, as well as some additional experiments. One semester was not enough to carry out all the ideas that came up when the experiments were performed. As all the final experiments had to be comparable to each other, the protocols could not be changed during the late stages of the work. Some suggestions to further investigations are listed here:

1. Too much PpIX in the cells plasma membranes may contribute to the high level of necrosis found in these experiments. There is a chance that by using regular cultivation medium instead of PBS while washing the cells before irradiation, some of the PpIX in the plasma membrane will be extracted. This could increase the probability of inducing apoptosis, as there would be less PpIX molecules incorporated in the plasma membrane, and therefore a lower probability of inducing direct cell membrane rupture.

2. The fractionation experiments should be repeated using lower doses — preferably a range of doses should be examined, making an interesting comparison to the continuous dose-response curves. Changes in shoulder width is one of the phenomena which could provide us with more information about the effects of PDT on the AY-27 cells, and about accumulation of sublethal damages.

3. Five minutes may be too short time for any repair processes in the cell to function properly, and longer dark intervals should be tested to look for the existence of an active sublethal damage repair in the AY-27 cell line after red light HAL-PDT.

4. Figure 5.8b indicates an early increase in cell size after HAL-PDT. It may be worthwhile to examine the response of the forward scattered signal in the flow cytometer by performing some osmosis experiments with the AY-27 cells to validate the understanding of the changes in FSC signal as changes in cell size.

Chapter 7

Conclusions

- HAL-PDT with our treatment conditions, 10 μM, 3.5 h, using red light of 630 nm and an irradiance of 20 mW/cm^2, induces necrosis as the dominant mode of cell death in the AY-27 cancer cell line.
- The LD_{50} dose one hour after treatment is 5.4 J/cm^2. 24 hours after treatment this is equivalent to a LD_{80} dose.
- No altered effect was detected between treatment with fractionated and continuous light delivery.
- The survival after split dose treatment seemed to depend on conditions before irradiation, but seems otherwise to give the same amount of cell death as fractionated or continous light delivery.
- Confocal microscopy examination of several samples, such as in a HAL-PDT dose-response experiment, is time consuming. Analysis of the results is even more time consuming, and I would therefore not recommend the use of confocal microscopy in quantitative studies of cell death after photodynamic therapy. It is however a powerful tool for studies of fluorescence localization and photobleaching, and thus well suited for qualitative studies of mechanisms activated after PDT .

Bibliography

[1] D. E. Dolmans, D. Fukumura, and R. K. Jain, "Photodynamic therapy of cancer," *Nature reviews cancer*, vol. 3, no. 5, pp. 380–387, 2003.

[2] A. Juzeniene, *Photodynamic therapy and Fluorescence diagnosis based on 5-aminolevulinic acid*. PhD thesis, UiO, 2007.

[3] A. Weyergang, *Photochemical internalization of epidermal growth factor receptor-targeted drugs*. PhD thesis, UiO, 2009.

[4] O. A. Gederaas, *Biological mechanisms involved in 5-aminovulinic acid based photodynamic therapy*. PhD thesis, NTNU, The Norwegian Radium Hospital, 2000.

[5] D. Parkin, F. Bray, J. Ferlay, and P. Pisani, "Estimating the world cancer burden: Globocan 2000," *International Journal of Cancer*, vol. 94, no. 2, pp. 153–156, 2001.

[6] B. Stewart and P. Kleihues, eds., *World cancer report*. Iarc, 2003.

[7] E. L. P. Larsen, L. L. Randeberg, O. A. Gederaas, C.-J. Arum, A. Hjelde, C.-M. Zhao, D. Chen, H. Krokan, and L. O. Svaasand, "Monitoring of hexyl 5-aminolevulinate-induced photodynamic therapy in rat bladder cancer by optical spectroscopy," *Journal of Biomedical Optics*, vol. 13, no. 4, 2008.

[8] D. Shackley, C. Whitehurst, J. Moore, N. George, C. Betts, and N. Clarke, "Light penetration in bladder tissue: implications for the intravesical photodynamic therapy of bladder tumours," *BJU international*, vol. 86, no. 6, pp. 638–643, 2000.

[9] P. N. Prasad, *Introduction to biophotonics*. John Wiley and Sons, Inc., Hoboken, New Jersey, 2003.

[10] L. O. Bjørn, ed., *Photobiology, The Science of Life and Light*, ch. 1, pp. 35–36. Springer, 2008.

[11] E. G. Milk, J. Stap, M. Sinaasappel, J. F. Beek, J. A. Aten, J. A. van Leeuwen, and C. Ince, "Mitochondrial PO_2 measured by delayed fluorescence of endogenous protoporphyrin IX," *Nature (Methods)*, vol. 3, pp. 939–945, 2006.

[12] A. Johnsson. Personal communication, 2008.

[13] L. B. Josefsen and R. W. Boyle, "Photodynamic therapy and the development of metal-based photosensitisers," *Metal-Based Drugs*, 2008.

[14] K. Berg, M. Folini, L. Prasmickaite, P. Selbo, A. Bonsted, B. Engesæter, N. Zaffaroni, A. Weyergang, D. A., G. Mælandsmo, E. Wagner, O. Norum, and A. Høgset, "Photochemical internalization: A new tool for drug delivery," *Current Pharmaceutical Biotechnology*, vol. 8, no. 6, pp. 1–11, 2007.

[15] K. Berg, P. Selbo, A. Weyergang, A. Dietze, L. Prasmickaite, A. Bonsted, B. . Engesæter, E. Petersen, T. Warloe, N. Frandsen, and A. Høgset, "Porphyrin-related photosensitizers for cancer imaging and therapeutic applications," *Journal of Microscopy*, vol. 218, no. 2, pp. 133–147, 2005.

[16] K. Plaetzer, T. Kiesslich, T. Verwanger, and B. Krammer, "The modes of cell death induced by PDT: An overview," *Medical Laser Application*, vol. 18, no. 1, pp. 7–19, 2003.

[17] L. Cekaite, Q. Peng, A. Reiner, S. Shahzidi, S. Tveito, I. E. Furre, and E. Hovig, "Mapping of oxidative stress responses of human tumor cells following photodynamic therapy using hexaminolevulinate," *BMC Genomics*, vol. 8, no. 273, 2007.

[18] W.-X. Zong and C. B.Thompson, "Necrotic death as a cell fate," *Genes and Development*, vol. 20, no. 1, pp. 1–15, 2006.

[19] G. Majno and I. Joris, "Apoptosis, oncosis, and necrosis. An overview of cell death," *American Journal of Pathology*, vol. 146, no. 1, pp. 3–15, 1995.

[20] S. L. Fink and B. T. Cookson, "Apoptosis, pyroptosis, and necrosis: Mechanistic description of dead and dying eukaryotic cells," *Infection and Immunity*, vol. 73, no. 4, pp. 1907–1916, 2005.

[21] H. Lecoeur, M.-C. Prévost, and M.-L. Gougeon, "Oncosis Is Associated With Exposure of Phosphatidylserine Residues on the Outside Layer of the Plasma Membrane: A Reconsideration of the Specificity of the Annexin V/Propidium Iodide Assay," *Cytometry*, vol. 44, no. 1, pp. 65–72, 2001.

[22] D. Voet, J. G. Voet, and C. W. Pratt, *Fundamentals of Biochemistry.* John Wiley and Sons, Inc, 2008.

[23] K. Plaetzer, T. Kiesslich, C. B. Oberdanner, and B. Krammer, "Apoptosis Following Photodynamic Tumor Therapy: Induction, Mechanisms and Detection," *Current Pharmaceutical Design*, vol. 11, no. 9, pp. 1151–1165, 2005.

[24] R. D. Almeida, B. J.Manadas, A. P. Carvalho, and C. B. Duarte, "Intracellular signaling mechanisms in photodynamic therapy," *BBA-Reviews on Cancer*, vol. 1704, no. 2, pp. 59–86, 2004.

[25] M. O. Li, M. R. Sarkisian, W. Z. Mehal, P. Rakic, and R. A. Flavell, "Phosphatidylserine Receptor is Required for Clearance of Apoptotic Cells," *Science*, vol. 302, pp. 1560–1563, 2003.

[26] D. Grebeňová, K. Kuželowá, K. Smetana, M. Pluskalová, H. Cajthamlová, O. F. Iuri Marinov, J. Souček, P. Jarolím, and Z. Hrkal, "Mitochondrial and endoplasmic reticulum stress-induced apoptotic pathways are activated by 5-aminolevulinic acid-based photodynamic therapy in HL-60 leukemia cells," *Journal of Photochemistry and Photobiology*, vol. 69, no. 2, pp. 71–85, 2003.

[27] I. Dalle-Donne, R. Rossi, D. Giustarini, A. Milzani, and R. Colombo, "Review. protein carbonyl groups as biomarkers of oxidative stress.," *Clinica Chimica Acta*, vol. 329, no. 1-2, pp. 23–28, 2003.

[28] P. A. Tsaytler, M. C. O'Flaherty, D. V. Sakharov, J. Krijgsveld, and M. R. Egmond, "Immediate protein targets of photodynamic treatment in carcinoma cells," *Journal of proteome research*, vol. 7, no. 9, pp. 3868–3878, 2008.

[29] S. Tanimoto, S. Matsamura, and K. Toshima, "Target-selective degradation of proteins by porphyrins upon visible photo-irradiation," *Chemical Communications*, 2008.

[30] B. Magi, A. Ettorre, S. Liberatori, L. Bini, M. Andreassi, S. Frosali, P. Neri, V. Pailini, and A. D. Stefano, "Selectivity of protein carbonylation in the apoptotic response to oxidative stress associated with photodynamic therapy: a cell biochemical and proteomic investigation," *Cell Death and Differentiation*, vol. 11, no. 8, pp. 842–852, 2004.

[31] I. K. Ekroll and M. B. Johnsen. Measurements performed in the subject TFY4 Optical Spectroscopy, 2008.

[32] Y. Ohgari, Y. Nakayasu, S. Kitajima, M. Sawamoto, H. Mori, O. Shimokawa, H. Matsui, and S. Taketani, "Mechanisms involved in δ-aminolevulinic acid (ALA)-induced photosensitivity of tumor cells: Relation of ferrochelatase and uptake of ALA to the accumulation of protoporphyrin," *Biochemical pharmacology*, vol. 71, no. 1-2, pp. 42–49, 2005.

[33] N. Schoenfeld, O. Epstein, M. Lahav, R. Mamet, M. Shaklai, and A. Atsmon, "The heme biosynthetic pathway in lymphocytes of patients with malignant lymphoproliferative disorders," *Cancer letters*, vol. 43, no. 1-2, pp. 43–48, 1988.

[34] Godal, N. O. Nilsen, J. Klaveness, J. E. Brænden, J. M. Nesland, and Q. Peng, "Photodynamic therapy: Chemical synthesis and porphyrin production in in vitro and in vivo biological systems," *Journal of Environmental Pathology*, vol. 25, no. 1-2, pp. 109–126, 2006.

[35] B. Kuitert, "Investigations of photoreactions in the cancer cell line AY-27, with special emphasis on reactive oxygen species," Master's thesis, NTNU, 2007.

[36] A. Juzeniene, K. P. Nielsen, and J. Moan, "Biophysical Aspects of Photodynamic Therapy," *Journal of Environmental Pathology, Toxicology and Oncology*, vol. 25, no. 1-2, pp. 7–28, 2006.

[37] A. P. Castano, T. N. Demidova, and M. R. Hamblin, "Mechanisms in photodynamic therapy: part two–cellular signaling, cell metabolism and modes of cell death," *Photodiagnosis and Photodynamic Therapy*, vol. 2, no. 1, pp. 1–23, 2005.

[38] E. J. Hall and A. J. Giaccia, *Radiobiology for the Radiologist*. Lippincott Williams & Wilkins, 6th ed., 2006.

[39] F. Stewart, P. Baas, and W. Star, "What does photodynamic therapy have to offer radiation oncologists (or their cancer patients)?," *Radiotherapy and Oncology*, vol. 48, pp. 233–248, 1998.

[40] H. Dertinger and H. Jung, *Molecular Radiation Biology*, ch. 2. Springer, 1969.

[41] A. Juzeniene, P. Juzenas, I. Bronshtein, A. Vorobey, and J. Moan, "The influence of temperature on photodynamic cell killing in vitro with 5-aminolevulinic acid," *Journal of Photochemistry and Photobiology*, vol. 84, pp. 161–166, 2006.

[42] T. Mosmann, "Rapid colorimetric assay for cellular growth and survival: Application to proliferation and cytotoxicity assays," *Journal of Immunological Methods*, vol. 65, no. 1-2, pp. 55–63, 1983.

[43] G. Denecker, H. Dooms, G. V. Loo, D. Vercammen, J. Grooten, W. Fiers, W. Declercq, and P. Vandenabeele, "Phosphatidyl serine exposure during apoptosis precedes release of cytochrome c and decrease in mitochondrial transmembrane potential," *FEBS letters*, vol. 465, pp. 47–52, 2000.

[44] C. de Lange Davies and B. Stokke, "Lecture notes TFY 4265 Biophysical Microtechniques."

[45] K. Sæterbø, "Dyrking av AY-27," Kvalitetshåndbok BS-504, NTNU, 2007-2009.

[46] C. B. Oberdanner, K. Plaetzer, T. Kiesslich, and B. Krammer, "Photodynamic treatment with fractionated light decreases production of reactive oxygen species and cytotoxicity in vitro via regeneration of glutathione," *Photochemistry and Photobiology*, vol. 81, pp. 609–613, 2005.

[47] I. K. Ekroll, "PDT induced cell death in the cancer cell line AY-27: Application of a method to detect possible protein oxidation after red light HAL-PDT." Specialization project in Biophysics, 2008.

[48] L. Helander. Unpublished results, 2008.

[49] A. Castano, T. Demidova, and M. Hamblin, "Mechanisms in photodynamic therapy: part one – photosensitizers, photochemistry and cellular localization," *PPT*, no. 1, pp. 279–293, 2004.

[50] A. Uzdensky, A. Juzeniene, L.-W. Ma, and J. Moan, "Photodynamic inhibition of enzymatic detachment of human cancer cells from a substratum," *BBA*, vol. 1670, pp. 1–11, 2004.

[51] A. Kamuhabwa, P. Agostinis, M. D'Hallewin, L. Baert, and P. de Witte, "Cellular photodestruction induced by hypericin in AY-27 rat bladder carcinoma cells," *Photochemistry and Photobiology*, vol. 74, no. 2, pp. 126–132, 2001.

[52] K. Plaetzer, T. Kiesslich, B. Krammer, and P. Hammerl, "Characterization of the cell death modes and the associated changes in cellular energy supply in response to $AlPcS_4$-PDT," *PPS*, no. 1, pp. 172–177, 2002.

[53] I. Furre, S. Shahzidi, Z. Luksiene, M. Moller, E. Borgen, J. Morgan, K. Tkacz-Stachowska, J. Nesland, and Q. Peng, "Targeting PBR by hexaminolevulinate-mediated photodynamic therapy induces apoptosis through translocation of apoptosis-inducing factor in human leukemia cells," 2005.

[54] L. Wyld, M. Reed, and N. Brown, "Differential cell death response to photodynamic therapy is dependent on dose and cell type.," *British journal of cancer*, vol. 84, no. 10, p. 1384, 2001.

[55] S. Smiley, M. Reers, C. Mottola-Hartshorn, M. Lin, A. Chen, T. Smith, G. Steele, and L. Chen, "Intracellular heterogeneity in mitochondrial membrane potentials revealed by a J-aggregate-forming lipophilic cation JC-1," *Proceedings of the National Academy of Sciences*, vol. 88, no. 9, pp. 3671–3675, 1991.

[56] V. Kielberg, N. Brünner, and P. Briand, eds., *Celledyrkning. En praktisk håndbog i dyrkning af mammale celler*. Gads forlag, 2001.

[57] P. M. Borell, P. Borell, and K. R. Grant, "Inverse temperature dependences in the quenching of singlet oxygen $O_2(^1\sum_g^+)$ by CO_2 and N_2O studied with a discharge flow/shock tube.," *J. Chem. Phys*, vol. 78, no. 2, pp. 748–756, 1983.

[58] M. Ascencio, J. P. Estevez, M. Delemer, M. O. Farine, P. Collinet, and S. Mordon, "Comparison of continuous and fractionated illumination during hexaminolaevulinate-photodynamic therapy," *Photodiagnosis and Photodynamic Therapy*, vol. 5, no. 3, pp. 210–216, 2008.

[59] P. Babilas, V. Schacht, G. Liebsch, O. Wolfbeis, M. Landthaler, R. Szeimies, and C. Abels, "Effects of light fractionation and different fluence rates on photodynamic therapy with 5-aminolaevulinic acid in vivo," *British journal of cancer*, vol. 88, no. 9, pp. 1462–1469, 2003.

[60] A. Curnow, J. Haller, and S. Bown, "Oxygen monitoring during 5-aminolaevulinic acid induced photodynamic therapy in normal rat colon Comparison of continuous and fractionated light regimes," *Journal of Photochemistry & Photobiology, B: Biology*, vol. 58, no. 2-3, pp. 149–155, 2000.

[61] H. de Bruijn, A. van der Ploeg-van den Heuvel, H. Sterenborg, and D. Robinson, "Fractionated illumination after topical application of 5-aminolevulinic acid on normal skin of hairless mice: The influence of the dark interval," *Journal of Photochemistry & Photobiology, B: Biology*, vol. 85, no. 3, pp. 184–190, 2006.

Appendix A

Miscellaneous information

A.1 The survival of AY-27 cells after HAL-PDT with different light irradiance

In the biophysics specialization project of fall 2008 [47], AY-27 cells were given HAL-PDT using the same light source as this semester, but with different irradiance. In the former study, an irradiance of 36 mW/cm^2 was used, while we used 20 mW/cm^2 in this year's studies. The survival curve is reproduced here for comparison with the results obtained in this study.

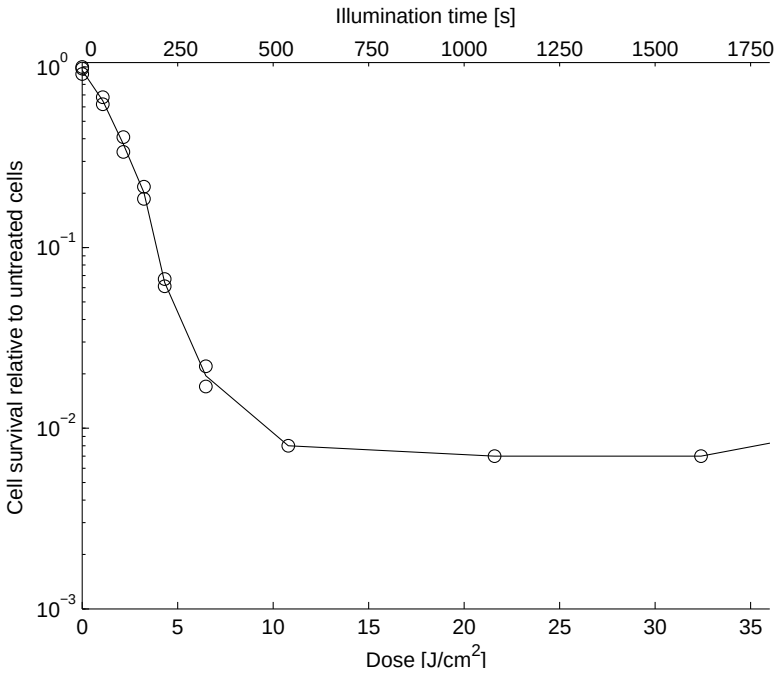

(a) Surviving fraction — semilog scale

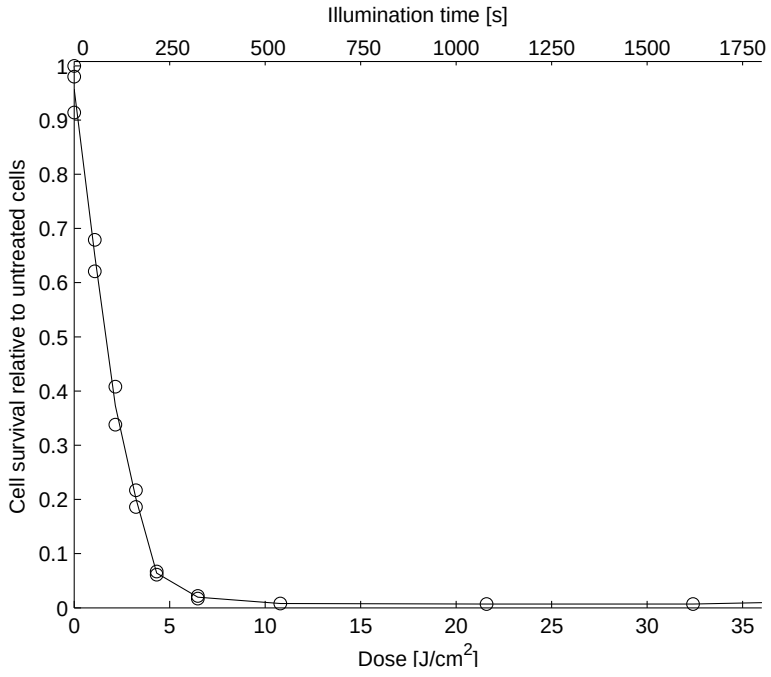

(b) Surviving fraction — linear scale

Figure A.1: The surviving fraction of AY-27 cells 24 hours after red light (630 nm, 36 mW/cm^2) HAL-PDT (3.5 h, 10 μM) measured by the MTT assay.

A.2 Typical MTT results from fractionation experiments

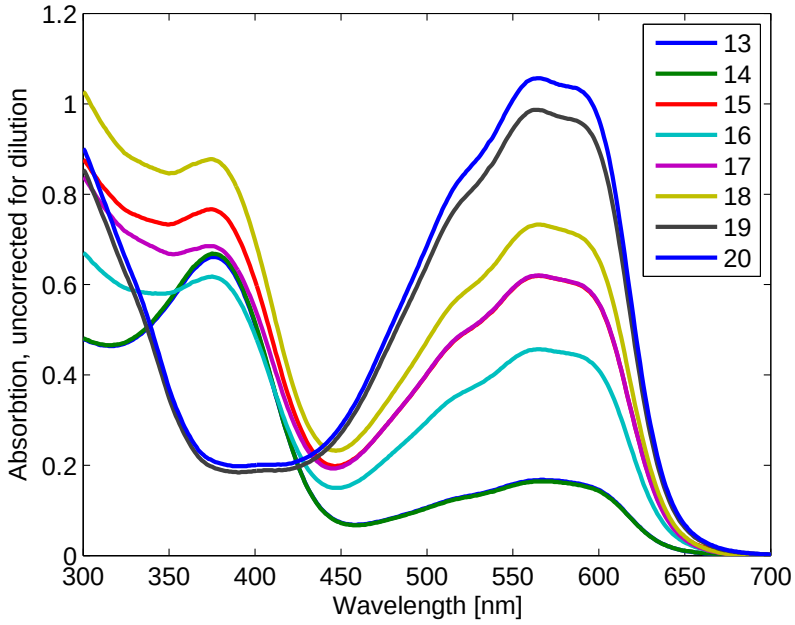

Figure A.2: Typical results from the spectrophotometric absorption measurements of the cell produced formazan dissolved in isopropanol 24 hours after HAL-PDT treatment. The absorption value at 595 nm is used to create bar charts for MTT results such as in Figure 5.11a. An overview of sample treatment is found in Table A.1. The high absorption in the treated samples around 400 nm may be due to PpIX present in the solution.

Table A.1: An overview of sample treatment during the MTT version of the fractionation experiments, where mitochondrial activity was measured 24 hours after HAL-PDT. (Samples 1-12 is used in flow cytometry studies 1 hour and 24 hours after treatment)

Sample	HAL	Irradiation	Light[s]/Dark[s]/Light[s]	Dilution
13	+	Split	135/300/135	1:1
14	+	Split	135/300/135	1:1
15	+	Frac	(45/60/45)x3	1:1
16	+	Frac	(45/60/45)x3	1:1
17	+	Cont	270/0/0	1:1
18	+	Cont	270/0/0	1:1
19	-	Control	0/0/0	1:10
20	-	Control	0/0/0	1:10

A.3 Contents of HEPES buffer

Table A.2: Contents of the HEPES buffer used in studies with the fluorochromes Ax and PI

Compound	**[g/l] in dH_2O**
Hepes (Sigma)	2.38
NaOH (Merck)	0.368
$CaCl_2$ (Merck)	0.550
NaCl	8.18

A.4 Settings of the flow cytometer

Table A.3: Settings of detectors and amplifiers in the flow cytometer when used with the fluorochromes Ax and PI

Param	**Detector**	**Voltage**	**AmpGain**	**FineGain**	**Laser**
P1 (FSC)	FSC-H		8	Off	1
P2 (SSC)	SSC-H	899	8	Off	1
P3 (Ax)	FL1-H	500	8	Off	1
P4	FL2-H	391	8	Off	1
P5	FL4-H	693	8	Off	2
P6	FL5-H	501	8	Off	2
P7	FL3-H	999	8	Off	1
P8 (PI)	FL6-H	800	8	Off	1
Threshold FSC:	54				

Table A.4: Compensation made when using the fluorochromes Ax/PI.

Detector	**Subtracts [%]**	**Of detector**
FL1 (Ax)	1.6	FL6 (PI)
FL6 (PI)	4.0	FL1 (Ax)